

MODELING OF CUTTING FORCES FOR PRECISION MILLING

by

HAYRİ BAKİOĞLU

Submitted to the Graduate School of Engineering and Natural Sciences
in partial fulfillment of the requirements for the degree of
Master of Sciences

Sabanci University

August 2015

MODELING OF CUTTING FORCES FOR PRECISION MILLING

APPROVED BY:

Prof. Erhan Budak
(Dissertation Supervisor)

Assoc. Prof. Bahattin Koç

Assoc. Prof. Mustafa Bakkal

DATE OF APPROVAL:

©Hayri Bakiođlu 2015

All Rights Reserved

ABSTRACT

Machining is one of the most frequently used techniques among other manufacturing methods. The developments on the machining have been continuing since the industrial revolution. Developments in micro and nano technologies led to a considerable increase in research efforts for manufacturing of these parts. Micro end milling operations have been one of the most widely used manufacturing method for producing these parts. As the tool radii are small and the tools are weaker than the ones in conventional milling, determination of cutting forces before the operation become an important consideration. The third deformation zone forces which are due to the hone radius at the cutting edge tip of the tool have a great contribution on the process mechanics as the uncut chip thicknesses are small.

The main aim of this thesis is to develop analytical models for micro end milling operations in order to be able to identify the cutting forces before the operation. Analytical models for the primary, secondary and third deformation zones are proposed. The third deformation zone forces and the bottom edge forces are also modeled with a mechanistic approach as well. All the proposed models are verified by experiments where reasonably good agreement is observed.

Keywords: Micro End Milling, Cutting Process Modeling, Third Deformation Zone, Cutting Forces

ÖZET

Talaşlı imalat, üretim teknikleri içerisinde en fazla sıklıkta kullanılanlardandır. Talaşlı imalat operasyonlarında sanayi devriminden bu yana süregelen bir gelişim gerçekleşmektedir. Mikro ve nano teknolojilerdeki gelişmeler, bu alanlar üzerine yapılan araştırmalarda ve parçaların üretimlerinde ciddi bir artışa olanak sağlamıştır. Mikro frezeleme operasyonları bu tarz parçaların üretilmesinde en yaygın olarak kullanılan tekniklerden bir tanesidir. Geleneksel frezeleme operasyonları ile karşılaştırılacak olursa, mikro frezeleme operasyonlarında kullanılan takımların çok daha ufak çaplarda ve daha kırılğan bir yapıya sahip olmaları, operasyon sırasında takım üzerine etkiyecek olan kuvvetlerin operasyondan önce tespit edilmesinin önemini dahada arttırmıştır. Mikro frezeleme operasyonlarındaki kesilmemiş talaş kalınlığı değerlerinin düşük olması, takım ucundaki radyüsten dolayı oluşan üçüncü deformasyon bölgesinin toplam kesme kuvvetleri üzerindeki payını arttırmıştır.

Bu tez çalışmasının ana amacı, mikro frezelemede oluşan kesme kuvvetlerinin operasyonlardan önce tespit edilmesi adına analitik ve mekanistik modeller oluşturulmasıdır. Birinci, ikinci ve üçüncü deformasyon bölgeleri için geliştirilen analitik modeller tanıtılmıştır. Bunun yanında yine üçüncü deformasyon bölgesi kuvvetleri ve takım tabanındaki sürtünme kuvvetleri deneysel olarak modellenmiştir. Önerilen modeller deneyler ile doğrulanmış, hesap edilen değerlerin deney sonuçları ile oldukça yakın olduğu görüşmüştür.

Anahtar Kelimeler: Mikro Frezeleme, Kesme Süreci Modellenmesi, Üçüncü Deformasyon Bölgesi, Kesme Kuvvetleri

ACKNOWLEDGEMENTS

First of all I am so thankful to my thesis advisor Prof. Erhan Budak who has always supported me on my thesis process. It was a great privilege and honor to work with him. I have learned a lot from his spectacular knowledge on cutting edge research. Not only his scientific guidance on my research, he has contributed a lot to my view of life.

I would also like to thank to the members of my jury committee Assoc. Prof. Bahattin Koc and Assoc. Prof. Mustafa Bakkal;

The members of Manufacturing Research Laboratory (MRL); especially Mehmet Albayrak, Umut Karagüzel, Samet Bilgen, Gözde Bulgurcu and Turgut Yalçın have always be patient and helpful on me during my master study.

I appritieate the assistance of the technicians of MRL; Ahmet Ergen, Tayfun Kalender, Atilla Balta, Esmâ Baytok, Anıl Sonugür, Süleyman Tutkun and Veli Nakşiler.

Finally, I am most thankful to my family, Mehmet and Berrin Bakiöglu for their sacrifices through my academic career. They have continuously supported my through my researches.

TABLE OF CONTENTS

1. INTRODUCTION	1
1.1. Introduction and Literature Survey	1
1.2. Objective	7
1.3. Layout of the Thesis	10
2. MODELING OF PRIMARY AND SECONDARY DEFORMATION ZONES BY THERMOMECHANICAL APPROACH.....	11
2.1. Modeling of Primary Deformation Zone	13
2.2. Two-Zone Contact Model and Orthogonal Cutting Approach for Micro End Milling Operations	14
2.3. The Forces Acting on the Regions	18
2.3.1. Region 1.....	18
2.3.2. Region 2.....	19
2.3.3. Region 3.....	21
2.4. Two-Zone Contact Model and Oblique Cutting Approach for Micro End Milling Operations	23
3. MODELING AND EXPERIMENTAL INVESTIGATION OF THIRD DEFORMATION ZONE IN ORTHOGONAL CUTTING AND MICRO – END MILLIG OPERATIONS.....	26
3.1. Thermo-mechanical Modeling of Third Deformation Zone Forces in Orthogonal Cutting	27

3.1.1.	The Forces Acting on Regions	31
3.1.1.1.	Region 4.....	31
3.1.1.2.	Region 5.....	33
3.1.1.3.	Region 6.....	35
3.2.	Experimental Verification of the Proposed Model of Third Deformation Zone 37	
3.3.	Experimental Modeling of Third Deformation Zone in Micro End Milling Operations.....	46
3.4.	Experimental Investigation of Third Deformation Zone Forces.....	46
4.	EXPERIMENTALLY INVESTIGATION OF THE BOTTOM EDGE FORCES IN MICRO END MILLING OPERATIONS	52
5.	WORKING AND VERIFICATION OF THE PROPOSED MODELS	55
5.1.	Working of Proposed Models	56
5.1.1.	Primary Deformation Zone.....	56
5.1.2.	Secondary Deformation Zone.....	57
5.1.3.	Third Deformation Zone.....	58
5.1.4.	Bottom Edge Forces	58
5.2.	The Experimental Verification.....	58
6.	SUGGESTIONS FOR FURTHER RESEARCH.....	62
7.	DISCUSSIONS AND CONCLUSIONS.....	64

LIST OF FIGURES

Figure 1 – Parameters for Milling Operations	2
Figure 2 – Slip-line field model of orthogonal micro cutting process [8]	4
Figure 3 – Trajectory of tool tip of micro end milling operations	5
Figure 4 – Trajectory of tool tip of Tlustý and Macneil’s model	5
Figure 5 – The three deformation zones for simple orthogonal cutting [22].....	11
Figure 6 – Axial Depth Elements	13
Figure 7 – Rake face of the cutting edge of the tool.....	15
Figure 8 – Stress distributions on rake face with sliding friction coefficient (a) larger than 1 and (b) less than 1 [22].....	15
Figure 9 – Illustration of cutting regions on rake face.....	17
Figure 10 – Normal and friction forces acting on Region 1	18
Figure 11 – Normal and friction forces acting on Region 2	20
Figure 12 – Normal and friction forces acting on Region 3	22
Figure 13 – Deformation Zones in orthogonal cutting [23].....	26
Figure 14 – Third Deformation Zone in Orthogonal Cutting Approach	28
Figure 15 – Cutting Regions in Third Deformation Zone [23].....	28
Figure 16 – Forces exerted on third deformation zone [23]	29

Figure 17 – Ploughing depth in third deformation zone	30
Figure 18 – Normal pressure distribution according to distance from the tool tip	30
Figure 19 – Normal and Friction forces acting on Region 4	32
Figure 20 – Normal and Friction Forces acting on Region 5	34
Figure 21 – Normal and Friction Forces acting on Region 6	35
Figure 22 – Feed vs Third deformation zone contact length at 250 m/min cutting speed	38
Figure 23 – Feed (mm/rev) vs total cutting forces (N) in tangential direction derived for the tools having 20, 40 and 60 micrometer hone radius at 250 m/min cutting speed.....	39
Figure 24 – Feed (mm/rev) vs total cutting forces (N) in feed direction derived for the tools having 20, 40 and 60 micrometer hone radius at 250 m/min cutting speed	39
Figure 25 – Hone Radius vs Edge forces in feed and tangential directions	40
Figure 26 – Hone radius (micm.) vs a and b	42
Figure 27 – Hone Radius (microm.) vs P_{MAX}/P_0	44
Figure 28 – Feed (mm/rev) vs tangential force F_t (N).....	45
Figure 29 – Feed (mm/rev) vs feed force F_f (N)	45
Figure 30 - Cutting Regions on the Flank Face	46
Figure 31 - Minimum Uncut Chip Thickness in Upmilling Operations.....	48
Figure 32 – KERN Evo Ultra Precision Machining Centre.....	49
Figure 33 – The Cutting Tool used in third deformation zone analysis	49

Figure 34 – Kistler Type 9256C	50
Figure 35 – Third Deformation Zone Analysis with 0.021 mm/rev*t feed, 6 mm diameter cutting tool, 5 degree helix angle, 2 mm axial depth of cut, 0.2 mm radial depth of cut, 5000 rpm spindle speed	51
Figure 36 – Feed per Tooth vs Feed (green lines) and Tangential (red lines) Forces at the stagnation angle	51
Figure 37 – (a) First experimental setup, bottom edge has no contact with the newly formed surface, (b) Second experiemntal setup, bottom edge has a contact with the newly formed surface.....	52
Figure 38 – Spindle Speed vs Ave. Diff. For Ffeed and Ftangential (f:0.008mm/rev*t)	54
Figure 39 – Spindle Speed vs Ave. Diff. For Ffeed and Ftangential (f:0.012mm/rev*t)	54
Figure 40 – Solution steps for proposed model	56
Figure 41 – Nanofocus Usurf.....	59
Figure 42 – Cutting test results for the forces in feed and tangential directions	59
Figure 43 – Feed (mm/rev*t) vs experiment and model results for the forces in feed and the tangential directions	60
Figure 44 – Feed (mm/rev*t) vs experiment and model results for the forces in feed and the tangential directions	60

LIST OF TABLES

Table 1 – Third deformation zone contact lengths derived experimentally for different hone radius tools, feeds and cutting speeds	37
Table 2 – Feed and Tangential Edge Force and contact lengths derived using full recovery approach.....	40
Table 3 – Feed and Tangential Edge Forces and contact lengths derived using partial recovery approach.....	41
Table 4 – Feed and tangential edge forces, the contact length constants a and b and predicted contact lengths	42
Table 5 – P _{MAX} / P ₀	43
Table 6 – Cutting Conditions for Third Deformation Zone Experiments.....	49
Table 7 – Third Deformation Zone Force Coefficients derived experimentally	51
Table 8 – Bottom Edge cutting coefficients	54
Table 9 – Johnson – Cook parameters for the proposed model for AISI 1050 steel	57

1. INTRODUCTION

1.1. Introduction and Literature Survey

Converting raw materials into the finished parts is one of the oldest methodologies in human history. At each era, people have used different methods to shape raw materials. The technological advances allow humans to shape in an easy and accurate way. The stones which were used as shapers in the Stone Age are replaced with cutting tools, the woods which were used as raw materials are replaced with steels. The Industrial Revolution has a significant contribution on the manufacturing processes. There are several manufacturing processes can be listed to shape materials in order to give them functionality. Some of the manufacturing methods can be summarized as casting, forging, forming, welding, machining etc.

Machining is one the most frequently used manufacturing technique among others. The final shape of the desired part is derived by removing unwanted material from the raw material by using cutting tools. The basics of the removing process depend on the hardness of the cutting tool which should be higher than the raw materials in order for cutting operation to take place. The machining processes can manufacture several types of materials such as metals, cast irons, ceramics, composites, polymers, rubber, thermoplastics etc. The cutting tools can be made of carbon steels, high speed steels, cast cobalt alloys, cemented carbides, ceramics, cermets, cubic boron nitride, diamond etc. The machining processes include milling, turning, drilling, tapping, boring, broaching.

Milling is one of the most commonly used processes in the industry. It is the machining process which uses rotary cutters to remove the unwanted material from the workpiece. Milling is used in a variety of applications which desire complex shaping while the cutting tool moves along multiple axes and require accuracy to have low tolerances. In milling; a cutter is held in a rotary spindle, while the workpiece is clamped on the table.

As the cutting tool moves linearly across the workpiece, the cutting process occurs. One of the important aspects of this cutting process is the trochoidal path of the cutting edge of the tool which is due to rotation of the spindle and linear motion of the axes. The cutting parameters in milling processes are: spindle speed which is generated by the spindle rotation, feed rate which is the velocity at which the tool is advanced against the workpiece, axial depth of cut which is the depth of the tool along its axis into the workpiece and radial depth of cut which is the depth of the tool along its radius into the workpiece. The parameters for milling process are illustrated on Figure 1 [1].

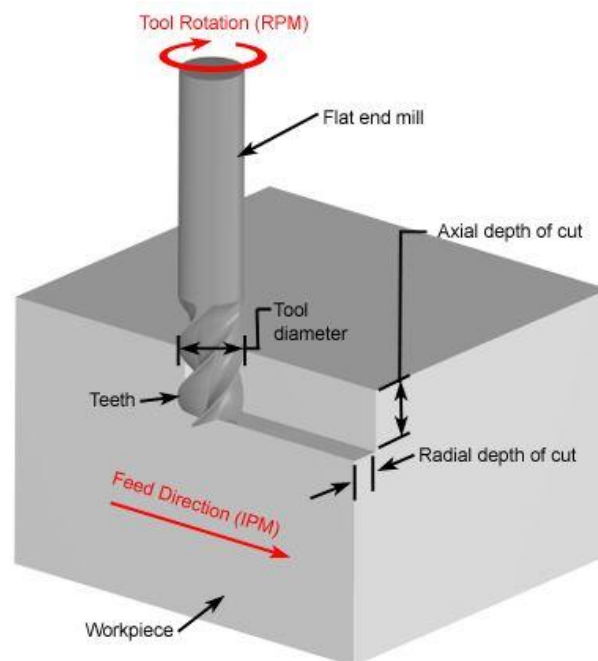


Figure 1 – Parameters for Milling Operations [1]

The main aim of this thesis is to develop analytical and mechanistic models to predict the cutting forces in micro end milling operations. The developed models are validated by cutting where reasonably good agreement is observed with the predictions and the test results. The developed models can be used for selecting the proper cutting parameters in industrial operations.

The milling process is considered as an interrupted cutting in which each tooth traces a trochoidal path [2,3]. The path of the cutting tooth creates a periodic but varying chip

thickness at each rotation [4]. The chip thickness in milling operation varies as a function of instantaneous immersion of the cutting edge which can be expressed as;

$$h(\varnothing) = c \sin \varnothing \quad (1.1)$$

where c is the feed rate (mm/rev.tooth) and \varnothing is the instantaneous angle of immersion [5].

The small tool diameters and uncut chip thicknesses are the main differences between micro milling and conventional milling operations. Because of that difference most of the process models developed for conventional milling operations are not applicable for micro scale. One of the most important considerations for micro end milling is the effect of hone radius [6]. Even though for the conventional milling, the effect of hone radius is neglected, for micro milling as the uncut chip thickness is small, the hone radius have a significant effect on the total cutting forces. In their work Bissacco *et al.* [7] developed a cutting force model considering the cutting edge radius size effect. The model depends on the experimental investigation on the effect of the edge radius in orthogonal cutting. In order to calculate the cutting forces for milling operation from orthogonal cutting, the engaged portion of the cutter is divided into a finite number of axial elements. On the other hand when we compare the micro milling operations with conventional milling, the material properties play a crucial role during the cutting process. As the cutting occurs in a small region, the material models used for conventional milling operations may not be applicable for micro scale operations.

In the literature there are several approaches that are used to model the cutting forces for micro end milling operations. One of the most frequently used approaches is the slip-line field theory. In their work Jin *et al.* [8] developed a slip-line field model to predict the cutting forces by dividing the material deformation region in the cutting process into three regions which are primary, secondary and third deformation zones. An illustration of slip-line field model for orthogonal model is shown in Figure 2.

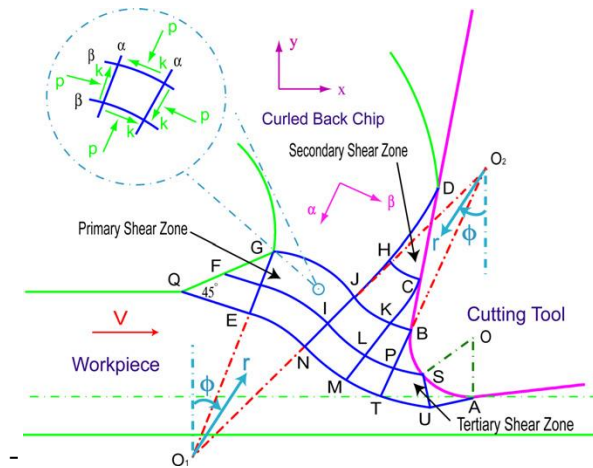


Figure 2 – Slip-line field model of orthogonal micro cutting process [8]

In his work Fang [9] developed a new slip-line field model for a rounded-edge cutting tool. The proposed model consists of 27 slip-line sub-regions and each sub-region has its own physical meaning. One limitation of the model is; it only applies on orthogonal metal cutting with continuous chip formation. The limitation is due to the assumption of the deformation of work material is under plane-strain conditions. In another work, Altintas *et al.* [10] presented an analytical prediction model for micro-milling forces from constitutive model of the material and friction. They used slip-line field theory to predict the chip formation process. The effect of the tool edge radius is included in the slip-line field model. The proposed model is verified by experiments made with 200 μm diameter cutting tool with 3.7 μm tool edge radius on workpiece with material Brass 260.

Mechanistic approaches are also used to model the cutting forces in micro end milling operations. Malekian *et al.* [11] used the mechanistic modeling approach for predicting micro end milling forces by considering the effects of ploughing, elastic recovery, run-out and dynamics. The critical chip thickness under which there is no chip formation occurs is obtained based on the edge radius and the experimentally derived cutting forces vs. feed rate curves. For the chip thickness values greater than the critical uncut chip thickness, conventional sharp-edge theorem is used to identify the cutting constants by performing curve fittings from the experimental data. For the chip thickness values less than the critical uncut chip thickness, a model for the ploughing-dominant cutting regime is considered and ploughing coefficients based on the ploughing area is

introduced. In their work Park *et al.* [12] worked on mechanistic modeling of shearing and ploughing domain cutting regimes to predict the cutting forces in micro end milling operations. In the model, the critical uncut chip thickness is defined and used to identify whether the cutting is predominantly shearing or ploughing. In another work, Bao [13] developed a new analytical cutting force model that calculates the uncut chip thickness by considering the trajectory of the tool tip. The trajectories of micro end milling tool and conventional end milling tools are illustrated on Figure 3 and Figure 4 respectively.

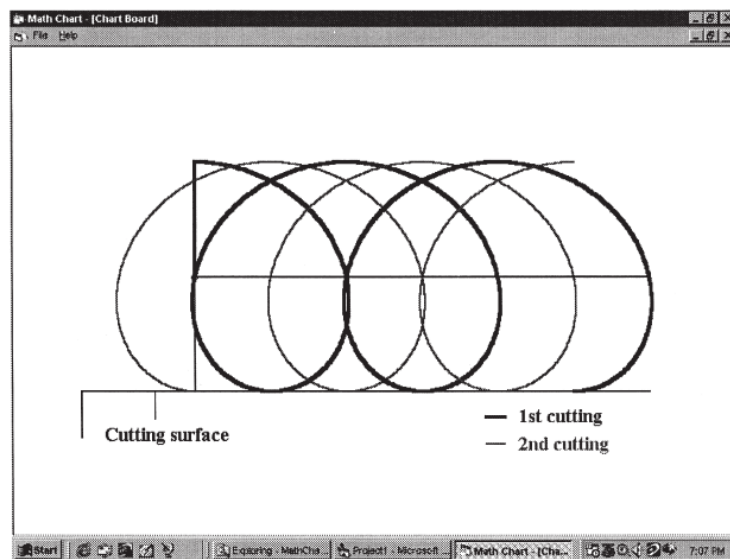


Figure 3 – Trajectory of tool tip of micro end milling operations

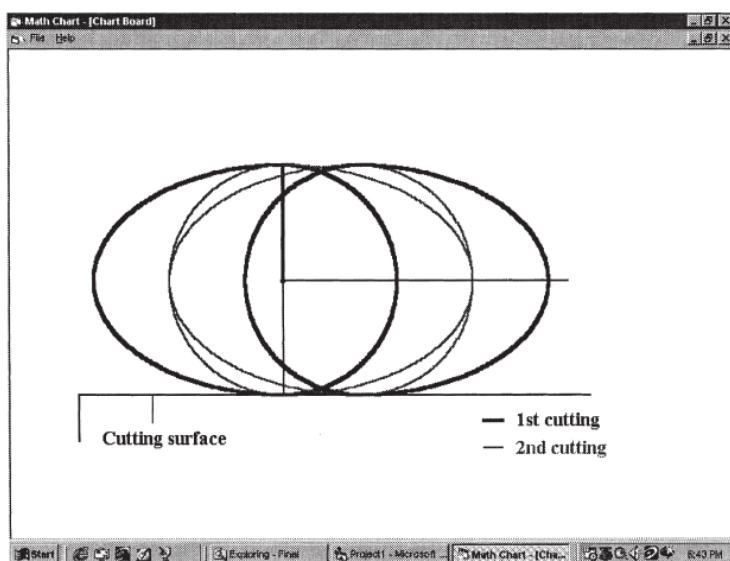


Figure 4 – Trajectory of tool tip of Tlustý and Macneil's model

Newby *et al.* [14] presented an empirical model for the analysis of cutting forces in micro end milling operations. In their work, they illustrated the true trochoidal nature of the tool edge path in the derivation of a chip thickness. The developed model proposes that the cutting force constant for tangential forces are of the same order of magnitude but the curvature is higher for micro end milling compared to conventional milling. On the other hand the cutting force constant for radial forces are of the same order of magnitude but the plot for cutting forces and feed are concave down for conventional milling whereas it is concave up for micro milling case. Zaman *et al.* [15] introduced a new approach to analytical three dimensional cutting forces modeling for micro end milling. The proposed model determines the theoretical chip area at any specific angular position of the tools cutting edge by considering the geometry of the path of the edge. The main assumptions of the proposed model are; instantaneous tangential component of the cutting force is proportional to the instantaneous chip area, instantaneous radial component of the cutting forces which is vertical component of instantaneous tangential forces, is proportional to the instantaneous tangential component of the cutting forces. One drawback of the model is; it assumes that the tool is perfectly sharp which neglects the third deformation zone forces. In their work Volger *et al.* [16] incorporated the critical uncut chip thickness concept in order to predict the effects of the cutter edge radius on the cutting forces. A slip-line plasticity force model is used to predict the cutting forces when the uncut chip thickness is greater than the critical uncut chip thickness value and an elastic deformation force model is used for the cases when the uncut chip thickness is less than critical uncut chip thickness.

Finite element is another approach that is frequently used to model and predict the cutting forces for micro end milling operations. In their work Afazov *et al.* [17] presented a new approach for prediction of cutting forces in micro end milling using finite-element method (FEM). There is an orthogonal finite element (FE) model developed which includes the run-out effects as well. The trajectory of the tools edge is modeled relative to radius of the tool, spindle angular velocity, run-out effect and feed rate. An orthogonal cutting is simulated in a dynamic thermo-mechanical finite element analysis program ABAQUS/Explicit. The advantage of the developed FE model is that it considers the material behavior at different plastic strains, strain rates and temperatures. In another work, Jin *et al.* [18] predicted the micro end milling cutting

forces from cutting forces coefficients obtained from FE simulations. The FE element simulations are made for an orthogonal micro cutting case with round edge cutting tool. The model is useful for illustrating the effect of tool edge geometry, uncut chip thickness and cutting speed on cutting forces. Lai *et al.* [19] also developed a FE model for micro scale orthogonal machining operations considering the material behavior by using a modified Johnson – Cook material model.

It is well known that in the flat end milling operations the bottom edge of the cutting tool is always in contact with the newly formed surface. Even though there is no chip formation occurs with respect to this contact, ploughing phenomena described for the third deformation zone occurs in this region and there appears a force as a result of this contact. In spite of there are lots of works have been done recently investigating the cutting forces in flat end milling operations, the bottom edge forces are a new area of study. In their work Dang *et al.* [20] investigated the contribution of flank edge and bottom edge contacts on total cutting forces. A mechanistic approach model is developed to characterize the contact on the bottom edge and it is observed that the influence of the bottom edge contact forces are not negligible and they can be treated as a linear function of bottom uncut chip width. In another work, Wan *et al.* [21] have proposed a mechanistic model to identify the bottom edge forces in flat end milling operations.

1.2. Objective

The tool diameters are relatively small and the tools are easier to be broken for micro end milling as we compare it with the larger diameter and stronger tools used for conventional milling operations. Thus, accurate modeling of cutting forces plays an important role for micro end milling operations. Selection of optimum process parameters for industrial and specific applications under cutting force consideration requires the modeling of cutting forces as well. Several process models and different modeling approaches have been reviewed in the previous section. Mechanistic approaches or curve fit models are widely used in the literature. The models developed with this approach might predict the cutting forces precisely for some specific cases; however they don't provide insight about the process mechanism. On the other hand

there is a large number of experiments should be made in order to calibrate the workpiece-cutting tool interaction for the calibration of cutting coefficients in order to develop a more accurate model. There are also studies can be found which are made with numerical analysis approaches. In those studies mostly the FEM (finite element method) or FDM (finite difference method) are used. The models made with this approach give detailed information about the cutting process and tool-workpiece interaction. However one drawback of these studies is the long solution times. In order to get the process simulation in more detail, the computation requires a lot of time which is not desired. On the other hand, if we consider a user who wants to find the optimum parameters in a certain range, it takes a lot of time to simulate and scan for the range. Models based on analytical or semi-analytical approaches such as slip-line field analysis are also frequently used in the literature. As we should consider these models are reasonably flexible in terms of modeling of the cutting region, there are numerous slip-line field analysis have been proposed and there is still no well accepted method for modeling the cutting operations. With regards to the previous works in the literature, the process models should present the cutting behavior in a precise way with fast and accurate computation. Our aim with this work is to propose process models to accurately calculate the cutting forces in micro end milling operations in a fast and accurate way. For this purpose thermo-mechanical approach is used for identifying the material behavior in the primary and secondary and third deformation zones. For the third deformation zone forces which have significant contribution on the total cutting forces, there is also a new experimental procedure is constituted to identify the cutting forces and the cutting coefficients which are due to the ploughing phenomena. As it was described earlier in [20,21] the contribution of bottom edge forces which are due to the contact between the bottom edge of flat end mill with the newly formed surface are not negligible. For this purpose, the bottom edge force coefficients are calibrated and added to the proposed models discussed earlier.

For the thermo-mechanical modeling of primary and secondary deformation zone, the proposed model developed by Ozlu *et al.* [22] for orthogonal cutting is applied to micro end milling application. Johnson-Cook constitutive material model is used to describe the material behavior in the primary deformation zone. The shear angle is predicted according to the minimum energy approach. The workpiece material parameters and

tool – workpiece interaction parameters are taken from [22]. The outputs of the proposed model are shear angle, shear stress, cutting forces in the secondary deformation zone, the stress distributions on the rake face of the cutting tool and the lengths of the sticking and sliding contact regions.

The third deformation zone forces which have a significant effect on the cutting forces as described earlier are another focus of the thesis. Third deformation zone forces are modeled according to the thermo-mechanical approach as well. Beside that; a new experimental procedure is applied to directly identify the third deformation zone forces from the experimental data. The comparison of the result of this new procedure is made with the thermo-mechanical model and regular linear regression analysis.

The bottom edge forces are identified throughout a series of experiments. Two series of experiments are made in order to clearly detect the effect of the bottom edge forces on total cutting forces. For the first experiments cutting tests are made when there the bottom edge of the cutting tool has no contact with the workpiece and later second experiments are made with regular slotting operation in which there is a contact between the bottom edge of the cutting tool and the newly formed surface. According to the experiment results, the bottom edge coefficients are calibrated.

1.3. Layout of the Thesis

The thesis is organized as follows;

In Chapter 2, thermo-mechanical approach used for the primary and secondary deformation zones are presented. Assumptions and formulations for calculation of the cutting forces due to the secondary deformation zone are given.

In Chapter 3, the proposed model for calculation of the third deformation zone forces are presented. A new experimental procedure for identifying the third deformation zone forces is described and comparison of new procedure results are made with proposed model and regular linear regression analysis.

In Chapter 4, the identification of the bottom edge forces are presented. The experimental results are discussed in detail and the derived cutting coefficients are given.

In Chapter 5, the results of the cutting force experiments are discussed and proposed models are verified by these experiment results.

In Chapter 6, the suggestions for the further research and conclusions are presented.

2. MODELING OF PRIMARY AND SECONDARY DEFORMATION ZONES BY THERMOMECHANICAL APPROACH

The modeling of the primary and secondary deformation zones on micro-end milling operations are one of the main objectives of this thesis. As it was discussed earlier, the uncut chip thickness values in micro end milling operations are relatively small when it is compared with the values in conventional end milling operations. Therefore most of the developed models for conventional milling are not applicable for micro end milling operations as they mostly neglect the hone radius at the cutting edge of the tool. The true representation of the cutting edge of the tool for a simple orthogonal cutting case is illustrated on Figure 5.

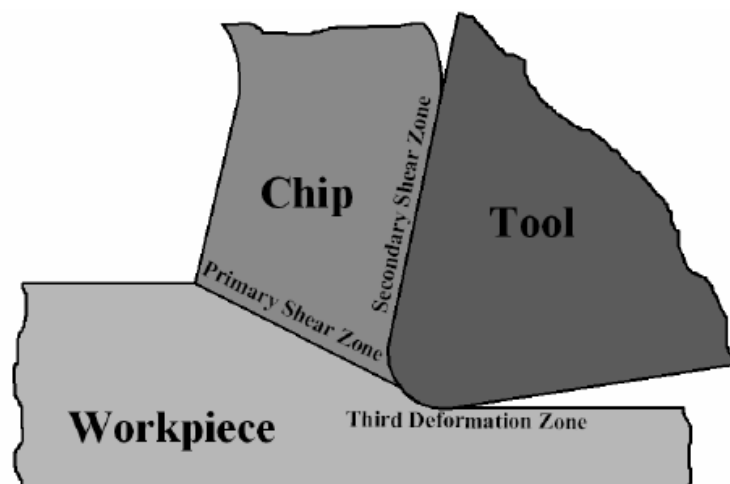


Figure 5 – The three deformation zones for simple orthogonal cutting [22]

A thermo-mechanical approach is applied on orthogonal and oblique cutting models while developing a micro end milling model.

As it was described earlier, the uncut chip thickness in milling operations varies as a function of immersion angle of the cutting edge of the tool. The relationship between the immersion angle and the actual uncut chip thickness is described in Equation (2.1).

$$h(\phi) = c \sin \phi \quad (2.1)$$

where c is the feed per tooth (mm/rev.tooth) and ϕ is the instantaneous angle of immersion [5]. On the other hand the helical structure of the cutting tools in milling operations causes a lag angle between each point on the cutting edge when we move on axial depth of cut. This lag angle changes the immersion angle of the cutting edge according to the axial position. The immersion angle of a cutting edge can be described as a function of axial position as;

$$\phi(z) = \phi - \frac{\tan \beta}{r} \cdot z \quad (2.2)$$

where “ z ” is the axial position of the cutting edge, β is the helix angle (rad.) and r is the radius of the cutting tool (mm). It can be observed from the above equations that the chip thickness varies according to the axial position. Because of that reason it is not applicable to use conventional orthogonal and oblique cutting models for milling operations. The lag angle should be considered during the modeling. For this purpose the axial cutting depth is divided into finite number of elements as shown in Figure 6.

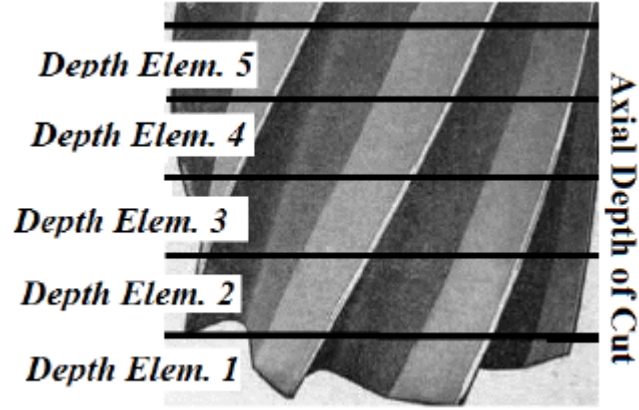


Figure 6 – Axial Depth Elements

The thermo-mechanical model is applied on each depth element which has different uncut chip thicknesses, separately and total cutting forces are calculated as sum of all of the cutting forces on each depth element.

In this chapter, the mathematical formulations of the proposed model are presented in detail. Firstly, the modeling of primary deformation zone is introduced, later the formulations for calculation of cutting forces in secondary deformation zone is introduced.

2.1. Modeling of Primary Deformation Zone

The primary deformation zone is modeled according to the work of Molinari *et al.* [24] and Dudzinski *et al.* [25]. The material behavior in the primary deformation zone is represented by Johnson – Cook constitutive model. The Johnson – Cook model is;

$$\tau = \frac{1}{\sqrt{3}} \left[A + B \left(\frac{\gamma}{\sqrt{3}} \right)^n \right] \left[1 + \ln \left(\frac{\dot{\gamma}}{\dot{\gamma}_0} \right)^m \right] [1 - (\bar{T})^v] \quad (2.3)$$

where γ is the shear strain, $\dot{\gamma}$ is the shear strain rate, $\dot{\gamma}_0$ is the reference shear strain rate, A , B , n , m and v are the material constants. \bar{T} is the reduced temperature and it can be calculated as;

$$\bar{T} = \frac{(T - T_R)}{(T_M - T_R)} \quad (2.4)$$

where T is the absolute temperature, T_R is the reference temperature and T_M is the melting temperature. The material entering the primary shear zone sustains a shear stress of τ_0 and the shear stress at the exit of the shear plane is τ_1 . Assuming a uniform pressure distribution along the shear plane, τ_0 can be iteratively calculated and using the principle of conservation of momentum, τ_1 can be obtained as;

$$\tau_1 = \rho (V \sin \phi)^2 \gamma_1 + \tau_0 \quad (2.5)$$

where ρ is the density of the workpiece material, γ_1 is the plastic shear strain at the exit of the primary deformation zone, V is the cutting speed and ϕ is the shear angle.

The assumptions that are made while modeling the primary deformation zone can be listed as;

- The primary shear zone has a constant thickness h .
- No plastic deformation occurs before and after the primary shear zone up to the sticking region on the rake face.
- There is a uniform pressure distribution along the shear plane.

The shear angle is also found iteratively according to the minimum energy shear angle principle.

2.2. Two-Zone Contact Model and Orthogonal Cutting Approach for Micro End Milling Operations

In this section, the dual zone contact model of Ozlu *et al.* [22] is formulated and introduced into the micro end milling operations. While introducing this model into milling operations, the cutting edge is divided with finite number of elements and the two – zone contact model is applied all of these depth elements individually. The rake

face of the cutting tool is divided into 3 sections while considering the hone radius. The representation of rake face is illustrated on Figure 7.

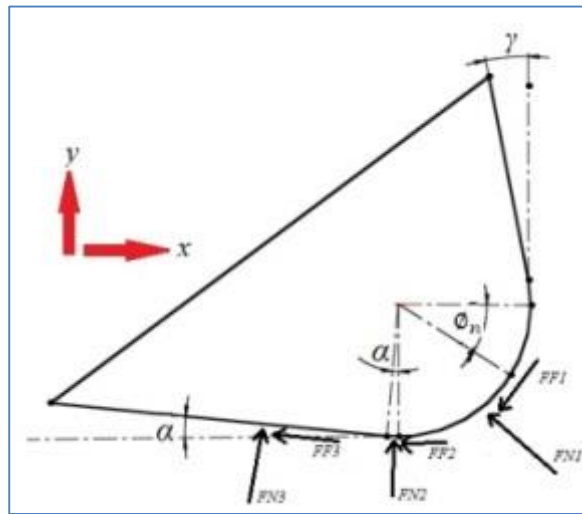


Figure 7 – Rake face of the cutting edge of the tool

The dual-zone contact model divides the rake face into 2 regions according to contact type between the cutting tool and chip. The contact might be sticking which is assumed to be a result of the high normal pressure at the exit of the primary deformation zone or sliding which is governed by Columb friction law appearing as a result of the decrease in the normal pressure. The stress distributions on the rake face and the sticking and sliding regions are illustrated on Figure 8.

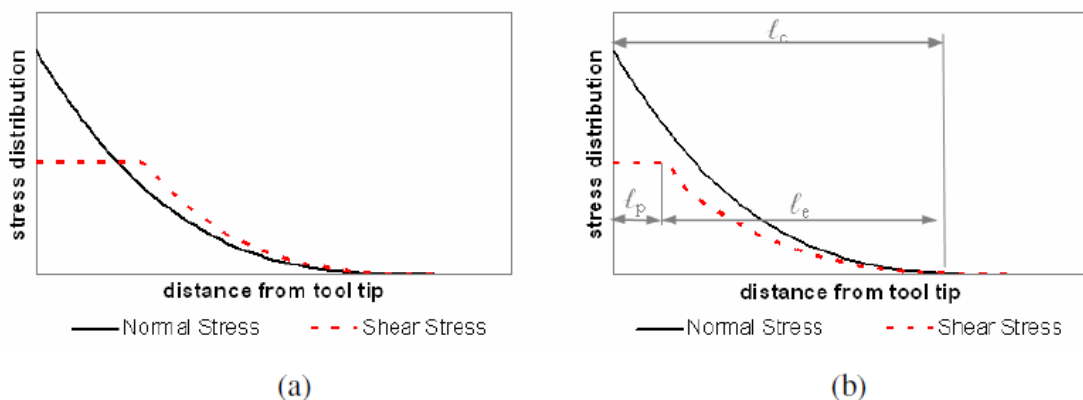


Figure 8 – Stress distributions on rake face with sliding friction coefficient (a) larger than 1 and (b) less than 1 [22]

The Figure 8 illustrates that P (normal pressure) decreases from the tool tip. The shear stress is formulated as;

$$\tau = \tau_1 \quad x \leq l_p \quad (2.6)$$

$$\tau = \mu P \quad l_p \leq x \leq l_c \quad (2.7)$$

where l_c is the total contact length between the tool and chip, x is the distance from the tool tip, l_p is the sticking zone contact length. The normal stress in Equation (2.7) varies with respect to the distance from the tool tip and can be calculated as;

$$P(x) = \mu P_0 \left(1 - \frac{x}{l_c}\right)^\zeta \quad (2.8)$$

When $P(x)$ is plugged into the Equation (2.7);

$$\tau_1 = \mu P_0 \left(1 - \frac{l_p}{l_c}\right)^\zeta \quad (2.9)$$

From Equation (2.9) sticking contact length l_p can be obtained as;

$$l_p = l_c \left(1 - \left(\frac{\tau_1}{P_0 \mu}\right)^{(1/\zeta)}\right) \quad (2.10)$$

The total contact length can be calculated as [22];

$$l_c = h_1 \frac{\zeta+2}{2} \frac{\sin(\phi+\lambda-\alpha)}{\sin \phi \cos \lambda} \quad (2.11)$$

The shear stress at the exit of the primary deformation zone is calculated as;

$$F_s = \tau_1 \frac{w h_1}{\sin \phi} \quad (2.12)$$

2.3. The Forces Acting on the Regions

In this part of the thesis each region illustrated on Figure 9 will be investigated individually. The formulations for calculation of the cutting forces action on each region will be described in detail.

2.3.1. Region 1

There are two forces which are the force in the normal direction and frictional force, are illustrated on Figure 10 [22].

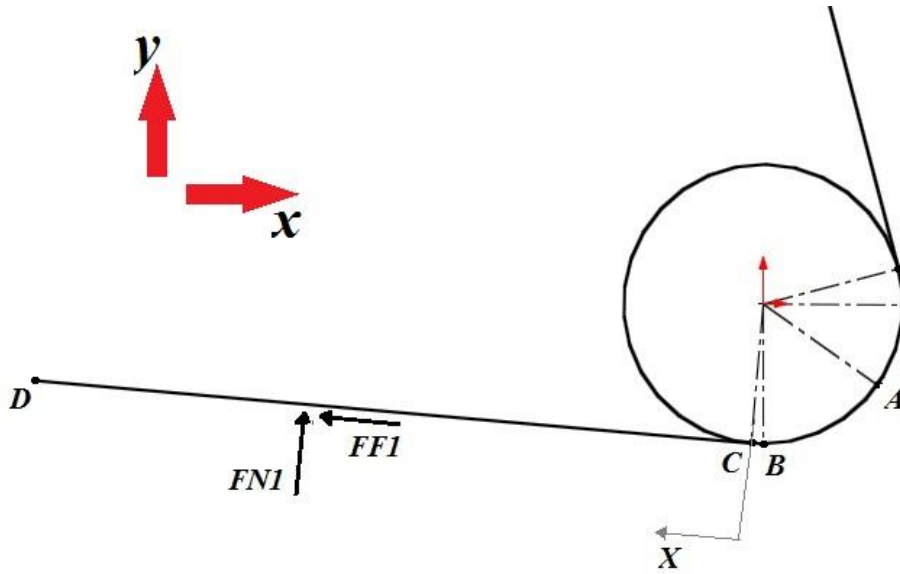


Figure 10 – Normal and friction forces acting on Region 1

The normal force acting on Region 1 can be defined as in [22] as;

$$F_{N1} = \int_{l_2+l_3}^{l_c} P_0 w \left(1 - \frac{x}{l_c}\right)^\zeta dx \quad (2.17)$$

where w is the depth of cut, ζ is the distribution exponent which is taken as 3 [22]. The components of the normal force in x and y direction are as follows;

$$F_{N1x} = F_{N1} \cdot \sin \alpha \quad (2.18)$$

$$F_{N1y} = F_{N1} \cdot \cos \alpha \quad (2.19)$$

As it is described in [22] the contact between the tool and the chip might be either sticking or sliding. For the friction force acting on Region 1, there may be two different cases. For the first case, the sticking zone contact length might be calculated as less than $l_2 + l_3$, and the contact on Region 1 might be only in sliding condition. For this case the friction force acting on Region 1 is defined as;

$$F_{F1} = \int_{l_2+l_3}^{l_c} \mu P_0 \left(1 - \frac{x}{l_c}\right)^\zeta dx \quad (2.20)$$

the x and y components of the friction force can be calculated as;

$$F_{F1x} = -F_{F1} \cdot \cos \alpha \quad (2.21)$$

$$F_{F1y} = F_{F1} \cdot \sin \alpha \quad (2.22)$$

For the second case, the sticking zone contact length might be calculated as higher than $l_2 + l_3$, and the contact on Region 1 might contain both sticking region which at the bottom of the Region 1 and sliding region which is after the sticking zone to end of the total contact length. For this case the friction force can be calculated as;

$$F_{F1} = \int_{l_2+l_3}^{l_p} \tau_1 w dx + \int_{l_p}^{l_c} \mu P_0 w \left(1 - \frac{x}{l_c}\right)^\zeta dx \quad (2.23)$$

the x and y components of the friction force can be calculated as;

$$F_{F1x} = -F_{F1} \cdot \cos \alpha \quad (2.24)$$

$$F_{F1y} = F_{F1} \cdot \sin \alpha \quad (2.25)$$

2.3.2. Region 2

The forces acting on Region 2 are illustrated on Figure 11 [22].

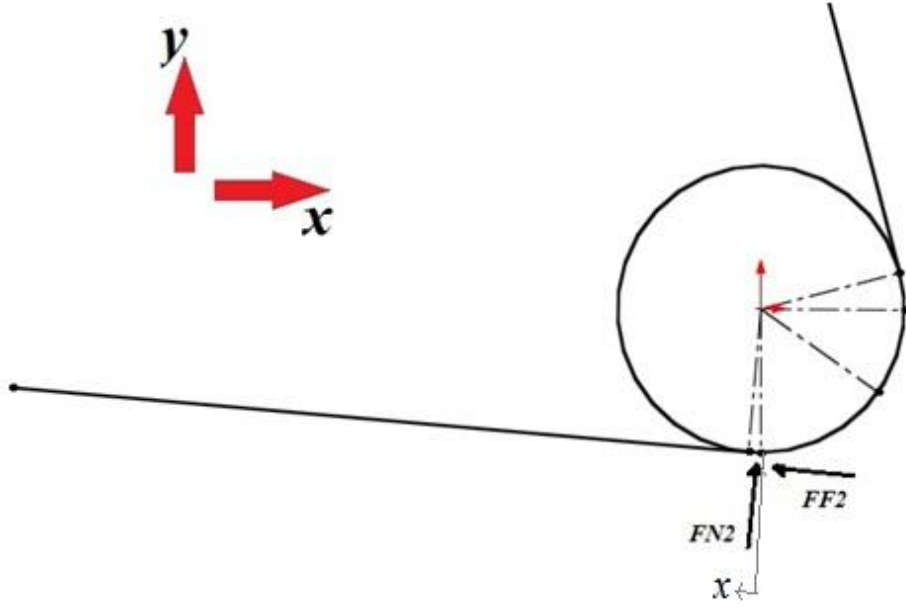


Figure 11 – Normal and friction forces acting on Region 2

As it can be observed from Figure 11, Region 2 is the area on the edge radius of the cutting tool. The normal forces acting on Region 2 on x and y directions can be calculated as;

$$F_{N2x} = \int_{l_2}^{l_2+l_3} P_0 w \left(1 - \frac{x}{l_c}\right)^\zeta \sin\left(\frac{x}{r} - \frac{\pi}{2} + \theta_s\right) dx \quad (2.26)$$

$$F_{N2y} = \int_{l_2}^{l_2+l_3} P_0 w \left(1 - \frac{x}{l_c}\right)^\zeta \cos\left(\frac{x}{r} - \frac{\pi}{2} + \theta_s\right) dx \quad (2.27)$$

For the friction force acting on the Region 2 there might be 3 different cases. For the first case sticking contact length might be less than l_3 ($l_p \leq l_3$) and the contact in Region 2 is only sliding. For this case the x and y components of the friction force can be defined as;

$$F_{F2x} = - \int_{l_3}^{l_2+l_3} \mu P_0 \left(1 - \frac{x}{l_c}\right)^\zeta \cos\left(\frac{x}{r} - \frac{\pi}{2} + \theta_s\right) dx \quad (2.28)$$

$$F_{F2y} = \int_{l_3}^{l_2+l_3} \mu P_0 \left(1 - \frac{x}{l_c}\right)^\zeta \sin\left(\frac{x}{r} - \frac{\pi}{2} + \theta_s\right) dx \quad (2.29)$$

For the second case the sticking zone might end in Region 2 which leads a sticking and sliding zones to appear in Region 2 at the same time. For this case x and y components of the friction force can be calculated as;

$$F_{F2x} = - \int_{l_3}^{l_p} \tau_1 w \cos\left(\frac{x}{r} - \frac{\pi}{2} + \theta_s\right) dx - \int_{l_p}^{l_2+l_3} \mu P_0 \left(1 - \frac{x}{l_c}\right)^\zeta \cos\left(\frac{x}{r} - \frac{\pi}{2} + \theta_s\right) dx \quad (2.30)$$

$$F_{F2y} = \int_{l_3}^{l_p} \tau_1 w \sin\left(\frac{x}{r} - \frac{\pi}{2} + \theta_s\right) dx + \int_{l_p}^{l_2+l_3} \mu P_0 \left(1 - \frac{x}{l_c}\right)^\zeta \sin\left(\frac{x}{r} - \frac{\pi}{2} + \theta_s\right) dx \quad (2.31)$$

For the third case the sticking zone contact length might be higher than l_p ($l_2 + l_3 \geq l_p$). For this case x and y components of the friction force can be calculated as;

$$F_{F2x} = - \int_{l_3}^{l_2+l_3} \tau_1 w \cos\left(\frac{x}{r} - \frac{\pi}{2} + \theta_s\right) dx \quad (2.32)$$

$$F_{F2y} = \int_{l_3}^{l_2+l_3} \tau_1 w \sin\left(\frac{x}{r} - \frac{\pi}{2} + \theta_s\right) dx \quad (2.33)$$

2.3.3. Region 3

The Region 3 as shown in Figure 9 is the first area after the stagnation point separating the secondary deformation zone from the third. The normal and friction forces acting on Region 3 are illustrated on Figure 12 [22];

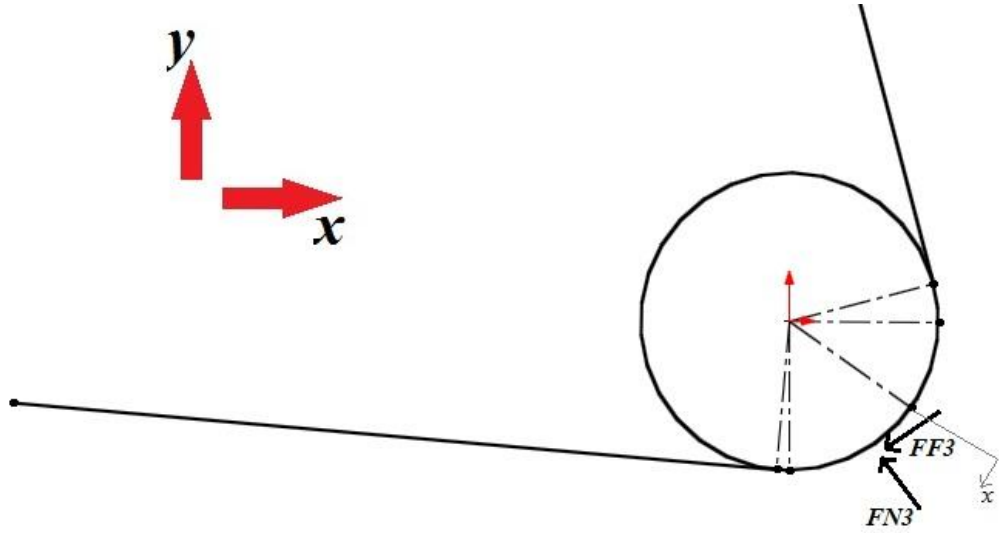


Figure 12 – Normal and friction forces acting on Region 3

The normal forces acting on Region 3 on x and y directions can be calculated as;

$$F_{N2x} = - \int_{l_2}^{l_2+l_3} P_0 w \left(1 - \frac{x}{l_c}\right)^\zeta \cos\left(\frac{x}{r} + \theta_s\right) dx \quad (2.34)$$

$$F_{N2y} = \int_{l_2}^{l_2+l_3} P_0 w \left(1 - \frac{x}{l_c}\right)^\zeta \sin\left(\frac{x}{r} + \theta_s\right) dx \quad (2.35)$$

For the friction force acting on this region there might be two different cases. For the first case, the sticking zone might end in Region 3 and the region might contain both sticking and sliding zones. For this case the components of the friction force on x and y direction can be calculated as;

$$F_{F3x} = - \int_0^{l_p} \tau_1 w \sin\left(\frac{x}{r} + \theta_s\right) dx - \int_{l_p}^{l_3} \mu P_0 \left(1 - \frac{x}{l_c}\right)^\zeta \sin\left(\frac{x}{r} + \theta_s\right) dx \quad (2.36)$$

$$F_{F3y} = - \int_0^{l_p} \tau_1 w \cos\left(\frac{x}{r} + \theta_s\right) dx - \int_{l_p}^{l_3} \mu P_0 \left(1 - \frac{x}{l_c}\right)^\zeta \cos\left(\frac{x}{r} + \theta_s\right) dx \quad (2.37)$$

For the second case, the sticking zone contact length might be higher than l_3 and the region might have only sticking contact. For this case the friction forces in x and y directions might be calculated as;

$$F_{F3x} = - \int_0^{l_3} \tau_1 w \sin\left(\frac{x}{r} + \theta_s\right) dx \quad (2.38)$$

$$F_{F3y} = - \int_0^{l_3} \tau_1 w \cos\left(\frac{x}{r} + \theta_s\right) dx \quad (2.39)$$

2.4. Two-Zone Contact Model and Oblique Cutting Approach for Micro End Milling Operations

The usage of two oblique cutting for micro end milling is similar with the orthogonal cutting approach. However the forces have components in z direction in oblique cutting. One important aspect for the oblique cutting model is the helix angle is taken as equal to the oblique angle for the model. The same division of axial depth of cut analogy is also applied for oblique cutting model. On the other hand, the rake face is also divided into 3 regions as shown in Figure 9.

The primary shear zone is modeled with Johnson-Cook material model as it was discussed earlier. The shear stress at the exit of the shear zone is calculated for the oblique model as [22];

$$\tau_1 = \rho (V \sin \phi \cos \lambda_s)^2 \gamma_1 + \tau_0 \quad (2.40)$$

where λ_s is the helix angle of the cutting tool. The only difference between the Equations (2.5) and (2.40) is the effect of helix angle.

The forces in the normal direction are calculated as;

$$F_{Ni} = \int_{l_i}^{l_{i+1}} P_0 w_c \left(1 - \frac{x}{l_c}\right)^\zeta dx \quad (2.41)$$

where w_c is the oblique depth of cut which is calculated as $(\cos \eta_c / \cos i)$ in which “ i ” is the helix angle and “ η_c ” is the chip flow angle. The chip flow angle is calculated by solving the following parabolic equation [22];

$$(A_1^2 + B_1^2)(\sin \eta_c)^4 - (2A_1C)(\sin \eta_c)^3 + 2(A_1C + CD) \sin \eta_c + (C^2 - B_1^2 - 2A_1^2 - 2A_1D)(\sin \eta_c)^2 + (A_1^2 + D^2 + 2A_1D) = 0 \quad (2.42)$$

where,

$$\begin{aligned} A_1 &= -\tan i (\tan \emptyset \sin \alpha + \cos \alpha) & B_1 &= \tan \emptyset \\ D &= \tan i \tan \beta (\cos \alpha \tan \emptyset - \sin \emptyset) & C &= \tan \lambda_a \end{aligned} \quad (2.43)$$

The total contact length on the rake face is calculated as [22];

$$l_c = h_1 \frac{\zeta+2}{2} \frac{\sin(\emptyset+\lambda-\alpha)}{\sin \emptyset \cos \lambda \cos \eta_c} \quad (2.44)$$

The shear stress and P_0 are also obtained as [22];

$$F_s = \tau_1 \frac{w h_1}{\sin \emptyset \cos i} \quad (2.45)$$

$$P_0 = \tau_1 \frac{h_1 (\zeta+1)}{l_c \sin \emptyset} \frac{\cos \lambda \cos \eta_s}{\cos(\emptyset + \lambda - \alpha) \cos \eta_c} \quad (2.46)$$

The shear flow angle is calculated as [22];

$$\eta_s = \tan^{-1} \left(\frac{(\tan i \cos(\emptyset - \alpha) - \tan \eta_c \sin \emptyset)}{\cos \alpha} \right) \quad (2.47)$$

The same division of the axial cutting depth approach is used for the oblique cutting model. The rake face is also divided into 3 regions. As the calculation of the force

components according to contact types are introduced in the previous section they are not going to be described in this section in detail.

3. MODELING AND EXPERIMENTAL INVESTIGATION OF THIRD DEFORMATION ZONE IN ORTHOGONAL CUTTING AND MICRO – END MILLIG OPERATIONS

Third deformation zone appears due to the edge radius at the tip of the cutting tool and the flank contact. Thus, the third deformation zone forces are as a result of the contact between the edge radius and flank edge of the cutting tool and the newly formed surface. Even though there is no chip formation in this region, some forces are exerted on the cutting tool due to the ploughing phenomena. The third deformation zone is illustrated on Figure 13 as the area between the points *A* and *C* where *A* is the stagnation point which separates the secondary deformation zone on the *rake face* from the third deformation zone.

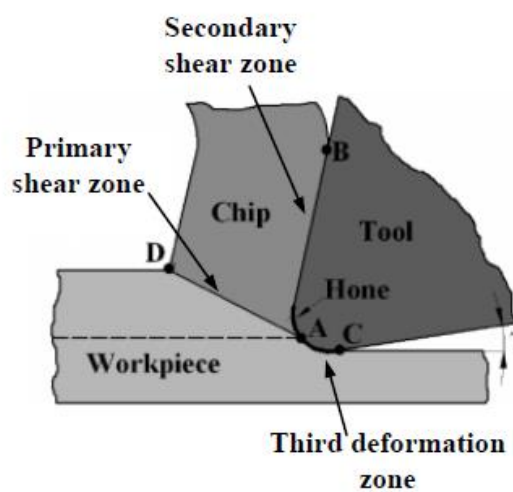


Figure 13 – Deformation Zones in orthogonal cutting [23]

Therefore it can be said that the forces exerted on the cutting tool have two components. The first components of the forces are due to the cutting on the rake face and the second component is due to the ploughing at the flank edge. Basically the cutting forces can be calculated as;

$$F_t = F_{tc} + F_{te} \quad (3.1)$$

$$F_f = F_{fc} + F_{fe} \quad (3.2)$$

where, F_f is the total forces in feed direction, F_t is the total forces in tangential direction, F_{fc} is the cutting force in feed direction, F_{tc} is the cutting force in tangential direction, F_{fe} is the edge force in feed direction and F_{te} is the edge force in tangential direction. The thermo-mechanical modeling of the forces in the secondary deformation zone which are due to the cutting process are described in the previous section. In this section, the thermo-mechanical model for the third deformation zone will be introduced for orthogonal cutting and a new experimental procedure will be given in order to detect the third deformation zone forces directly from a single experimental data.

3.1. Thermo-mechanical Modeling of Third Deformation Zone Forces in Orthogonal Cutting

In this section of the thesis, the thermo-mechanical modeling approach is introduced into the global orthogonal cutting. The third deformation zone for orthogonal cutting is illustrated on Figure 14.

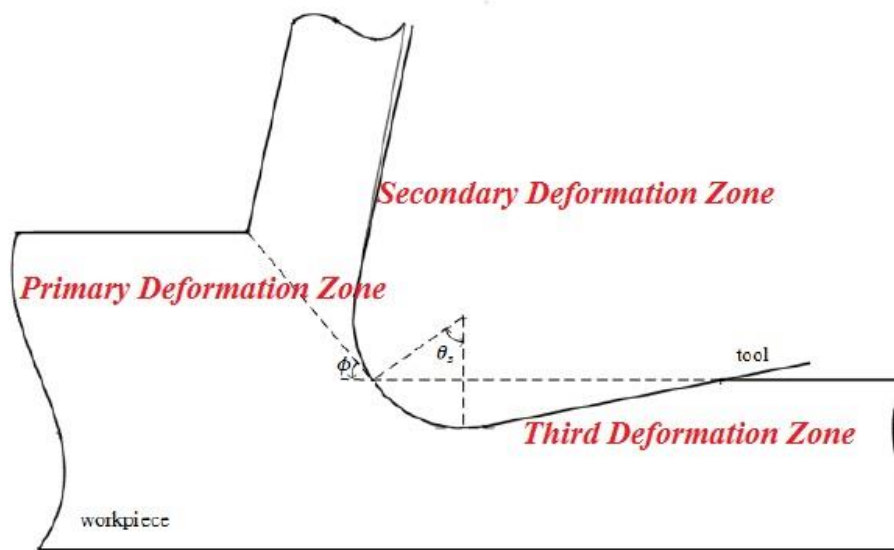


Figure 14 – Third Deformation Zone in Orthogonal Cutting Approach

As it was introduced in the previous section, the third deformation zone is divided into three regions as well. These three regions on the cutting tip are illustrated on Figure 15.

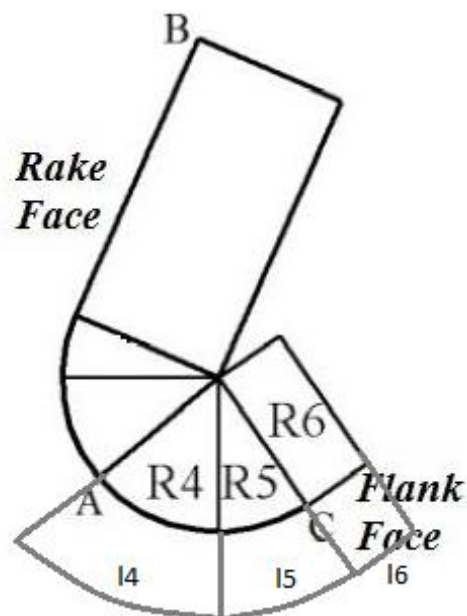


Figure 15 – Cutting Regions in Third Deformation Zone [23]

The contact lengths on each region are calculated as follows;

$$l_4 = r * \theta_s \quad (3.3)$$

$$l_5 = r * \gamma \quad (3.4)$$

$$l_6 = l_{c_{third_zone}} - (l_4 + l_5) \quad (3.5)$$

The boundary conditions for the third deformation zone are derived from the primary and secondary deformation zone model. The shear stress at the exit of the primary deformation zone is derived as in equation (2.5). The forces exerted on each region illustrated on Figure 15 are as in Figure 16.

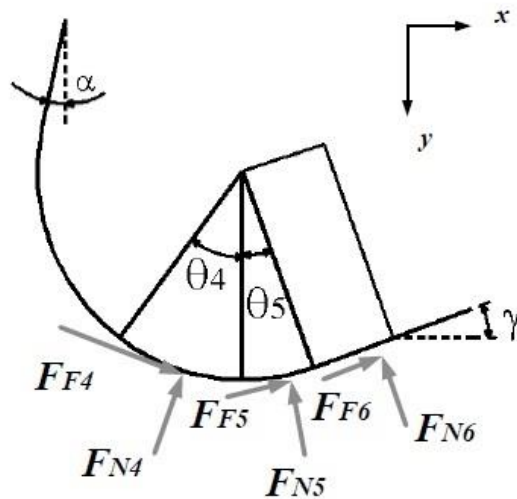


Figure 16 – Forces exerted on third deformation zone [23]

The dual-zone contact model which was also described in the previous section is used in the third deformation zone analysis. The contact between the tool and the workpiece might be sticking which is due to the high normal pressure or sliding which appears as a result of the decrease on the normal pressure. For the third deformation zone, the normal pressure is assumed to change as a function of ploughing depth which is illustrated as the shaded area on Figure 17.

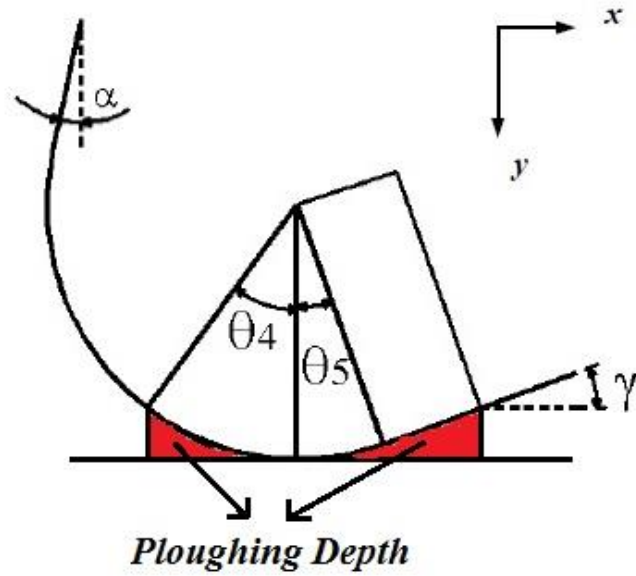


Figure 17 – Ploughing depth in third deformation zone

The change on the normal pressure as a function of distance from the tool tip is illustrated on Figure 18.



Figure 18 – Normal pressure distribution according to distance from the tool tip

While modeling the normal pressure distribution on the flank face, there were various types of relationships analyzed. From the experimental results in [22] and [23], it was

observed the normal pressure distribution on the flank face as a function of distance from tool tip is best fit by using a second order parabolic type equation as in (3.6);

$$P3(x) = a x^2 + b x + c \quad (3.6)$$

in which;

$$a = \frac{\left(\left(\frac{P_0 * l_{c_{third_zone}}}{l_4} \right) - P_0 \left(\frac{P_{MAX} * l_{c_{third_zone}}}{l_4} \right) \right)}{(l_{c_{third_zone}}^2 - (l_c * l_4))} \quad (3.7)$$

$$b = \frac{P_{MAX}}{l_4} - (a * l_4) - \left(\frac{P_0}{l_4} \right) \quad (3.8)$$

$$c = P_0 \quad (3.9)$$

and x is the distance from the tool tip.

The sticking zone contact length can be calculated as in equation (2.10).

3.1.1. The Forces Acting on Regions

In this part of the thesis each region illustrated on Figure 16 will be investigated individually. The friction and normal forces exerted on each region will be calculated.

3.1.1.1. Region 4

The Region 4 is the first area on the flank contact. The normal pressure is relatively higher in this region due to the compression of the material in the ploughing depth. The forces exerted on the cutting tool due to the contact in the Region 4 are as in Figure 19.

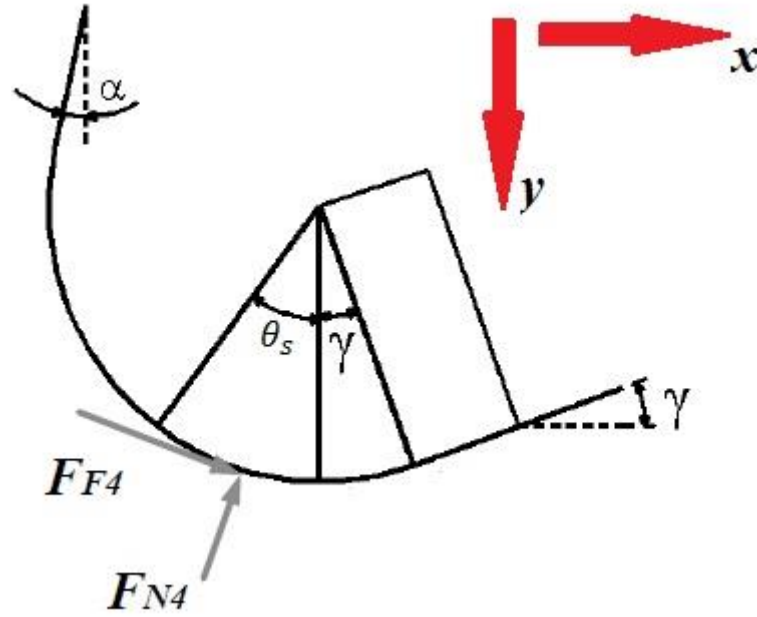


Figure 19 – Normal and Friction forces acting on Region 4

The normal forces acting on Region 4 are calculated as;

$$F_{N4X} = \int_0^{l_4} w * P3(x) \cos\left(\frac{\pi}{2} + \frac{x}{r} - \theta_s\right) dx \quad (3.10)$$

$$F_{N4Y} = -\int_0^{l_4} w * P3(x) \sin\left(\frac{\pi}{2} + \frac{x}{r} - \theta_s\right) dx \quad (3.11)$$

in which w is the axial depth of cut and $P3(x)$ is the normal pressure distribution derived as in equation (3.6).

For the friction forces there might be 3 different cases occur in the region. For the first case, the sticking contact length might be equal to zero and the friction forces are only due to the sliding contact. For this case the friction can be calculated as follows;

$$F_{F4X} = \int_0^{l_4} \mu * P3(x) * \sin\left(\frac{\pi}{2} + \frac{x}{r} - \theta_s\right) dx \quad (3.12)$$

$$F_{F4Y} = \int_0^{l_4} \mu * P3(x) * \cos\left(\frac{\pi}{2} + \frac{x}{r} - \theta_s\right) dx \quad (3.13)$$

in which μ is the sliding friction coefficient derived while modeling the secondary deformation zone.

For the second case, the sticking zone contact length might be higher than l_4 and the friction forces exerted on the region might be only due to the sticking contact. For this case the friction forces can be calculated as;

$$F_{F4X} = \int_0^{l_4} \tau_1 * w * \sin\left(\frac{\pi}{2} + \frac{x}{r} - \theta_s\right) dx \quad (3.14)$$

$$F_{F4Y} = \int_0^{l_4} \tau_1 * w * \cos\left(\frac{\pi}{2} + \frac{x}{r} - \theta_s\right) dx \quad (3.15)$$

For the third case, the sticking contact length might be higher than 0 and less than l_4 and the friction forces acting on the region might be sticking until the end of the sticking zone length and sliding from the end of the sticking region to l_4 . For this case, the friction forces can be calculated as;

$$F_{F4X} = \int_0^{l_{pthirdzone}} \tau_1 * w * \sin\left(\frac{\pi}{2} + \frac{x}{r} - \theta_s\right) dx + \int_{l_{pthirdzone}}^{l_4} \mu * P3(x) * \sin\left(\frac{\pi}{2} + \frac{x}{r} - \theta_s\right) dx \quad (3.16)$$

$$F_{F4Y} = \int_0^{l_{pthirdzone}} \tau_1 * w * \cos\left(\frac{\pi}{2} + \frac{x}{r} - \theta_s\right) dx + \int_{l_{pthirdzone}}^{l_4} \mu * P3(x) * \cos\left(\frac{\pi}{2} + \frac{x}{r} - \theta_s\right) dx \quad (3.17)$$

3.1.1.2. Region 5

Region 5 is the second area which is defined by the clearance angle at the tool hone, on the flank face. The forces exerted on the region are illustrated on Figure 20.

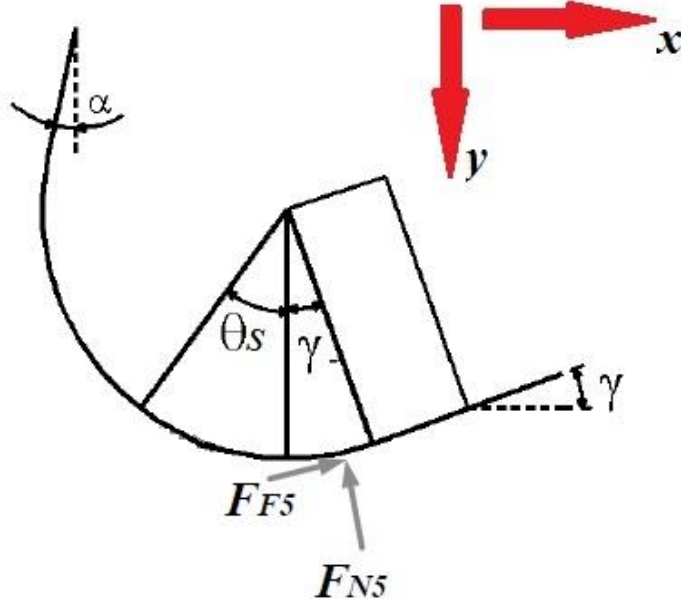


Figure 20 – Normal and Friction Forces acting on Region 5

The normal forces acting on Region 5 are calculated as;

$$F_{N5X} = - \int_{l_4}^{l_4+l_5} w * P3(x) \sin\left(\frac{x}{r} - \theta_s\right) dx \quad (3.18)$$

$$F_{N5Y} = - \int_{l_4}^{l_4+l_5} w * P3(x) \cos\left(\frac{x}{r} - \theta_s\right) dx \quad (3.19)$$

For the friction forces there might appear 3 different cases as well. For the first case, the sticking zone contact length might be less than l_4 and the friction forces acting on the region might be due to only sliding friction. For this case, the friction forces are calculated as;

$$F_{F5X} = \int_{l_4}^{l_4+l_5} \mu * P3(x) * \cos\left(\frac{x}{r} - \theta_s\right) dx \quad (3.20)$$

$$F_{F5Y} = - \int_{l_4}^{l_4+l_5} \mu * P3(x) * \sin\left(\frac{x}{r} - \theta_s\right) dx \quad (3.21)$$

For the second case the sticking zone contact length might higher than $(l_4 + l_5)$ and the friction forces acting on the region might only be due to sticking contact. The friction forces for this case are calculated as;

$$F_{F5X} = \int_{l_4}^{l_4+l_5} \tau_1 * w * \cos\left(\frac{x}{r} - \theta_s\right) dx \quad (3.22)$$

$$F_{F5Y} = - \int_{l_4}^{l_4+l_5} \tau_1 * w * \sin\left(\frac{x}{r} - \theta_s\right) dx \quad (3.23)$$

For the third case the sticking zone contact length might be higher than l_4 and less than $(l_4 + l_5)$. The friction forces acting on the region might be due to both sticking and sliding contact. The friction forces for this case can be calculated as;

$$F_{F5X} = \int_{l_4}^{l_{p\text{thirdzone}}} \tau_1 * w * \cos\left(\frac{x}{r} - \theta_s\right) dx + \int_{l_{p\text{thirdzone}}}^{l_4+l_5} \mu * P3(x) * \cos\left(\frac{x}{r} - \theta_s\right) dx \quad (3.24)$$

$$F_{F5Y} = - \int_{l_4}^{l_{p\text{thirdzone}}} \tau_1 * w * \sin\left(\frac{x}{r} - \theta_s\right) dx - \int_{l_{p\text{thirdzone}}}^{l_4+l_5} \mu * P3(x) * \sin\left(\frac{x}{r} - \theta_s\right) dx \quad (3.25)$$

3.1.1.3. Region 6

Region 6 is the last region on th flank contact. The forces acting on the region are illustrated on

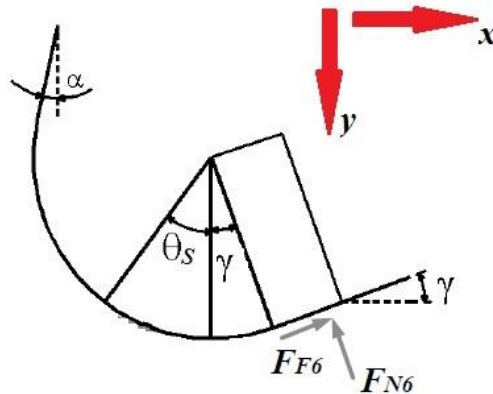


Figure 21 – Normal and Friction Forces acting on Region 6

The normal forces acting on Region 6 are calculated as;

$$F_{N6X} = - \int_{l_4+l_5}^{l_{c_thirdzone}} w * P3(x) \sin(\gamma) dx \quad (3.26)$$

$$F_{N6Y} = - \int_{l_4+l_5}^{l_{c_thirdzone}} w * P3(x) \cos(\gamma) dx \quad (3.27)$$

For the friction forces there might appear 3 different cases due to the sticking zone contact length. For the first case the sticking zone contact length might be less than $(l_4 + l_5)$ and the friction forces acting on the region might be only as a result of sliding contact. For this case, the friction forces are calculated as;

$$F_{F6X} = \int_{l_4+l_5}^{l_{c_thirdzone}} \mu * P3(x) * \cos(\gamma) dx \quad (3.28)$$

$$F_{F6Y} = - \int_{l_4+l_5}^{l_{c_thirdzone}} \mu * P3(x) * \sin(\gamma) dx \quad (3.29)$$

For the second case, the contact in the third deformation zone might be only sticking. For this case, the friction forces in the region can be calculated as;

$$F_{F6X} = \int_{l_4+l_5}^{l_{c_thirdzone}} \tau_1 * w * \cos(\gamma) dx \quad (3.30)$$

$$F_{F6Y} = - \int_{l_4+l_5}^{l_{c_thirdzone}} \tau_1 * w * \sin(\gamma) dx \quad (3.31)$$

For the third case, the sticking zone contact length might be higher than $(l_4 + l_5)$ and the friction forces might be due to both sticking and sliding contact. For this case, the friction forces are calculated as;

$$F_{F6X} = \int_{l_4+l_5}^{l_{p_thirdzone}} \tau_1 * w * \cos(\gamma) dx + \int_{l_{p_thirdzone}}^{l_{c_thirdzone}} \mu * P3(x) * \cos(\gamma) dx \quad (3.32)$$

$$F_{F6Y} = - \int_{l_4+l_5}^{l_{p_{thirdzone}}} \tau_1 * w * \sin(\gamma) dx - \int_{l_{p_{thirdzone}}}^{l_{c_{thirdzone}}} \mu * P3(x) * \sin(\gamma) dx \quad (3.33)$$

3.2. Experimental Verification of the Proposed Model of Third Deformation Zone

As it was described earlier in the objective part, one of the aims of the present work is to model and predict the forces which are due to the third deformation zone contact. In this chapter of the thesis the proposed model for the third deformation zone is introduced and in this part of the chapter the proposed model is verified experimentally for the orthogonal cutting approach. In the following parts the formulated third deformation model will be used for micro end milling operations. Before introducing the experiment results the contact length analysis for the third deformation zone will be illustrated. The contact length test results are taken from the work of Celebi *et al.* [23]. The experiments are conducted with a coated cutting tool having 3 degree clearance angle. The workpiece material is AISI 1050 steel. The contact lengths derived from the experiments are as in Table 1

Hone Radius(microm.)	Feed (mm/rev)	Cutting Speed (m/min)	Contact Length (microm.)
60	0,2	250	147
60	0,15	250	116
60	0,1	250	114
40	0,2	250	98,8
40	0,15	250	89,64
40	0,1	250	92,83
30	0,2	250	57
30	0,15	250	60
30	0,1	250	70
20	0,2	250	62,48
20	0,15	250	74,32
20	0,1	250	79,83

Table 1 – Third deformation zone contact lengths derived from experiments for different hone radius tools, feeds and cutting speeds

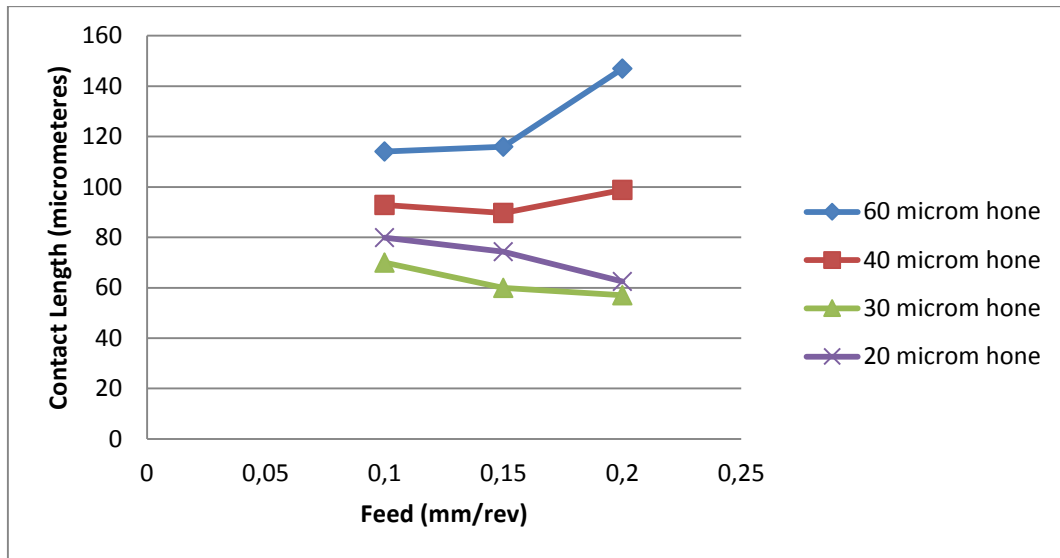


Figure 22 – Feed (mm/rev) vs Third deformation zone contact length (microm.) at 250 m/min cutting speed

From the experimental results it is observed that the contact length on the flank face for the large honed tools (40 and 60 micrometers) increase with the increasing feed however for the small honed tools (20 and 30 micrometers) the contact length decrease with the increasing feed. After the contact length analysis, the third deformation zone forces are also derived experimentally for different cases. The total cutting forces in tangential and feed direction are derived from orthogonal tube tests and illustrated on Figure 23 and Figure 24 respectively.

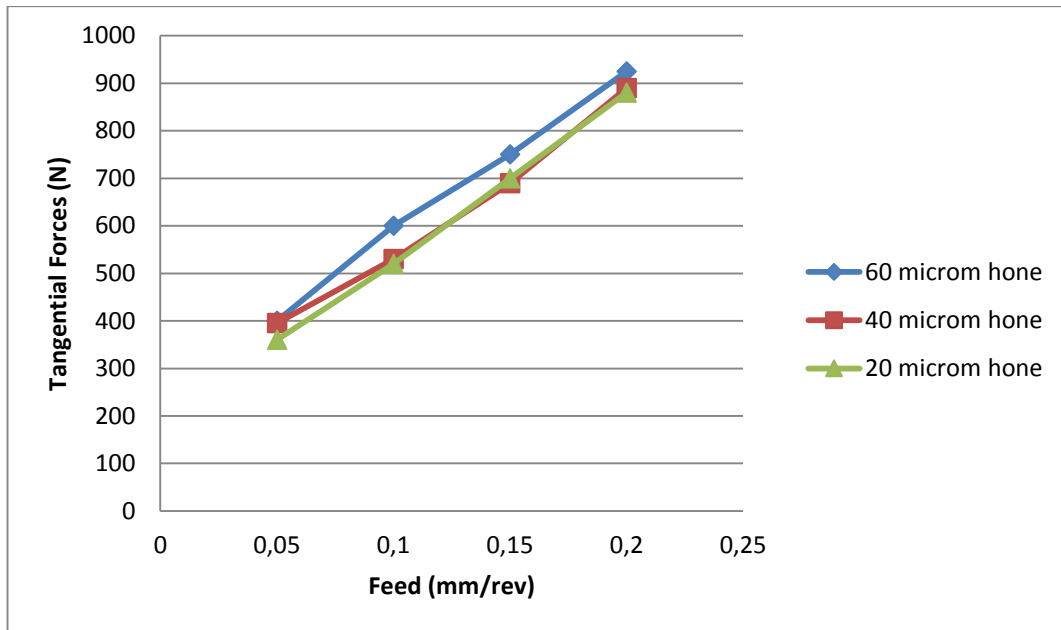


Figure 23 – Feed (mm/rev) vs total cutting forces (N) in tangential direction derived for the tools having 20, 40 and 60 micrometer hone radius at 250 m/min cutting speed

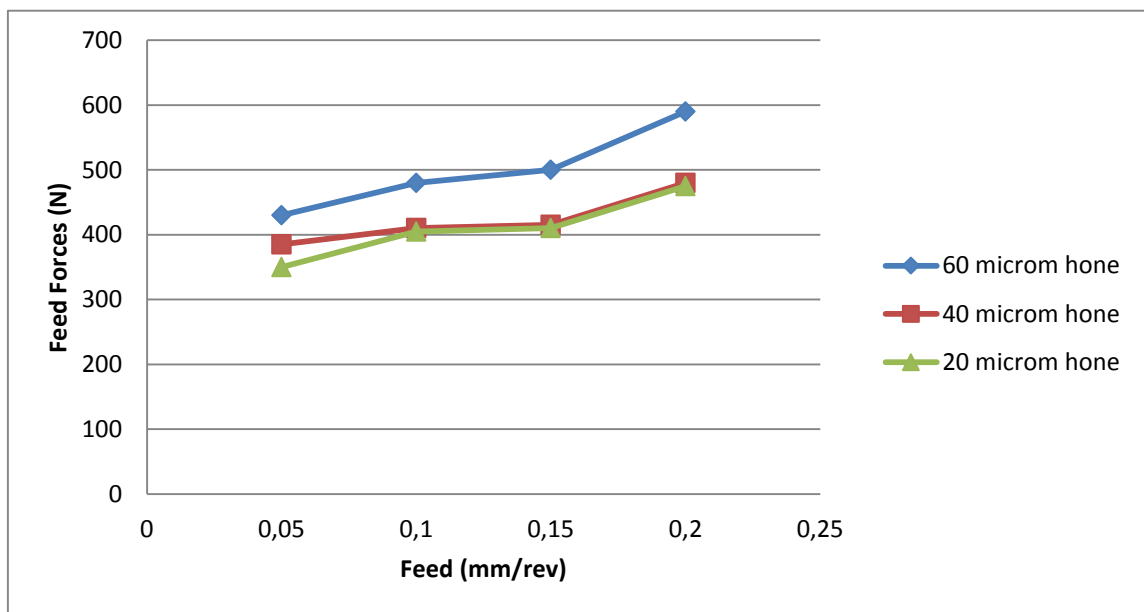


Figure 24 – Feed (mm/rev) vs total cutting forces (N) in feed direction derived for the tools having 20, 40 and 60 micrometer hone radius at 250 m/min cutting speed

The edge forces are calculated by extrapolating the total cutting forces derived in the experiments to 0 feed. The third deformation zone forces in tangential and feed direction are illustrated on Figure 25.

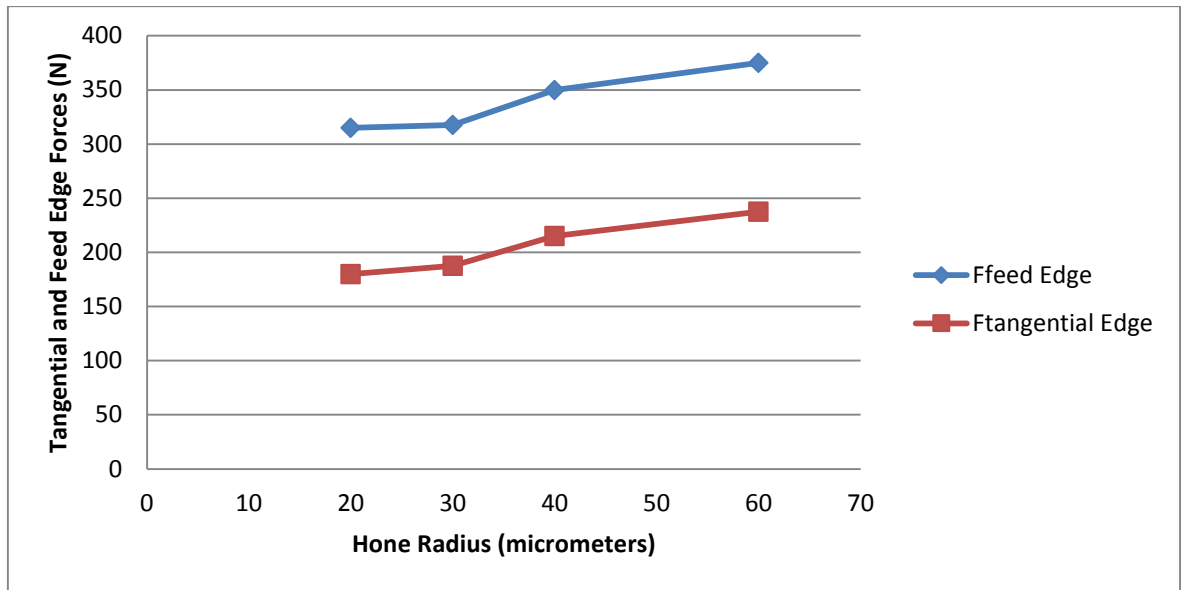


Figure 25 – Hone Radius (microm.) vs Edge forces (N) in feed and tangential directions

The next step is modeling the third deformation zone contact length. For this purpose two different approaches have been used. The first approach is full recovery case in which the material under the stagnation point is fully recovered. The contact lengths derived with this approach are illustrated on Table 2;

Hone(micm.)	f (mm/rev)	Ff Exp. (N)	Ft Exp. (N)	Con. L. Exp. (micm.)	Ff mod. (N)	Ft mod (N)	Con. L. mod (micm.)
60	0,2	-375	237,5	147	-847,9663678	510,6522614	209
60	0,15	-375	237,5	116	-770,4868878	466,9583889	186
60	0,1	-375	237,5	114	-709,2664971	391,6787854	144
40	0,2	-350	215	98,8	-568,7599277	331,7764329	132
40	0,15	-350	215	89,64	-545,6385934	326,4161637	132
40	0,1	-350	215	92,83	-513,6579252	311,3055926	124
30	0,2	-317,5	187,45	57	-411,0417586	236,0460125	98,8
30	0,15	-317,5	187,45	60	-428,8683034	249,5512213	98,8
30	0,1	-317,5	187,45	70	-432,2313669	258,3250846	104
20	0,2	-315	180	62,48	-302,9402216	168,3077912	65,9
20	0,15	-315	180	74,32	-298,5600181	168,306365	65,9
20	0,1	-315	180	79,83	-290,604901	167,8161808	65,9

Table 2 – Feed and Tangential Edge Force and contact lengths derived using full recovery approach

The next approach that is used for predicting the third deformation zone contact length is partial recovery approach in which the material under the stagnation point is partially recovered. The edge forces and contact lengths are derived as in Table 3 when the

partial recovery approach is used for predicting the third deformation zone contact length.

Hone(micm.)	f (mm/rev)	Ff Exp. (N)	Ft Exp. (N)	Con. L. Exp. (micm.)	Ff mod. (N)	Ft mod (N)	Con. L. mod (micm.)
60	0,2	-375	237,5	147	-181,2576618	165,2944094	52,1
60	0,15	-375	237,5	116	-176,4816657	160,9365041	46,5
60	0,1	-375	237,5	114	-181,9606179	161,274604	36
40	0,2	-350	215	98,8	-126,2699488	111,6368945	32,8
40	0,15	-350	215	89,64	-120,6906602	109,1260669	32,8
40	0,1	-350	215	92,83	-117,6544438	107,2910028	31
30	0,2	-317,5	187,45	57	-94,84300535	82,46538566	24,6
30	0,15	-317,5	187,45	60	-95,24989002	84,02455741	24,6
30	0,1	-317,5	187,45	70	-92,50758129	83,78169521	26
20	0,2	-315	180	62,48	-67,69782182	57,35844738	16,4
20	0,15	-315	180	74,32	-66,59772141	57,13943443	16,4
20	0,1	-315	180	79,83	-64,61937329	56,6179534	16,4

Table 3 – Feed and Tangential Edge Forces and contact lengths derived using partial recovery approach

It can clearly be seen from the Table 2 and Table 3 that the contact length predictions have some discrepancies with the experimental results. For the full recovery approach even though the model works well for small hone radiused tools, it have large discrepancy for the large hone radiused tools. On the other hand, for partial recovery approach even though the model works well for large hone radiused tools, the contact lengths for small hone radiused tools are found relatively small when it is compared with the model results. Therefore, for third deformation zone contact length prediction the combination of these two approaches described above will be used. The contact length will be determined as a function of hone radius of the cutting tool. The contact length have two components; the first one is due to the full recovery approach and the second one is due to the partial recovery approach. The contact length is determined as a function of hone radius as;

$$Contact\ Length = \frac{a*FullRec.CL+b*PartialRec.CL}{2} \quad (3.34)$$

The *Full Recovery Contact Length* and *Partial Recovery Contact Length* values are derived as in Table 2 and Table 3. The *a* and *b* values are the partition constants for *Recovery Contact Length* and *Partial Recovery Contact Lengths* respectively. The *a* and *b* constants are calibrated with the experiments as in

Hone (micm.)	f (mm/rev)	Ff Exp. (N)	Ft Exp. (N)	Con. L. Exp. (micm.)	Ff mod. (N)	Ft mod (N)	a	b	Con. L. mod (micm.)
60	0,2	-375	237,5	147	-370,0514205	253,9594406	1,2475	0,7525	149,96
60	0,15	-375	237,5	116	-336,7373053	233,0288103	1,2475	0,7525	133,51
60	0,1	-375	237,5	114	-288,3375106	197,9762962	1,2475	0,7525	103,365
40	0,2	-350	215	98,8	-351,5870399	218,6474694	1,27	0,73	95,762
40	0,15	-350	215	89,64	-337,0512746	214,8602526	1,27	0,73	95,762
40	0,1	-350	215	92,83	-317,3603379	204,9617506	1,27	0,73	90,055
30	0,2	-317,5	187,45	57	-324,8180907	192,2202246	1,0066	0,9933	61,94733
30	0,15	-317,5	187,45	60	-316,1526639	190,8810251	1,0066	0,9933	61,94735
30	0,1	-317,5	187,45	70	-298,2298097	186,3413528	1,0066	0,9933	65,20001
20	0,2	-315	180	62,48	-302,9402216	168,3077912	2	0	64,66
20	0,15	-315	180	74,32	-298,5600181	168,306365	2	0	64,66
20	0,1	-315	180	79,83	-290,604901	167,8161808	2	0	64,66

Table 4 – Feed and tangential edge forces, the contact length constants a and b and predicted contact lengths

The a and b values vs hone radius is illustrated on Figure 26.

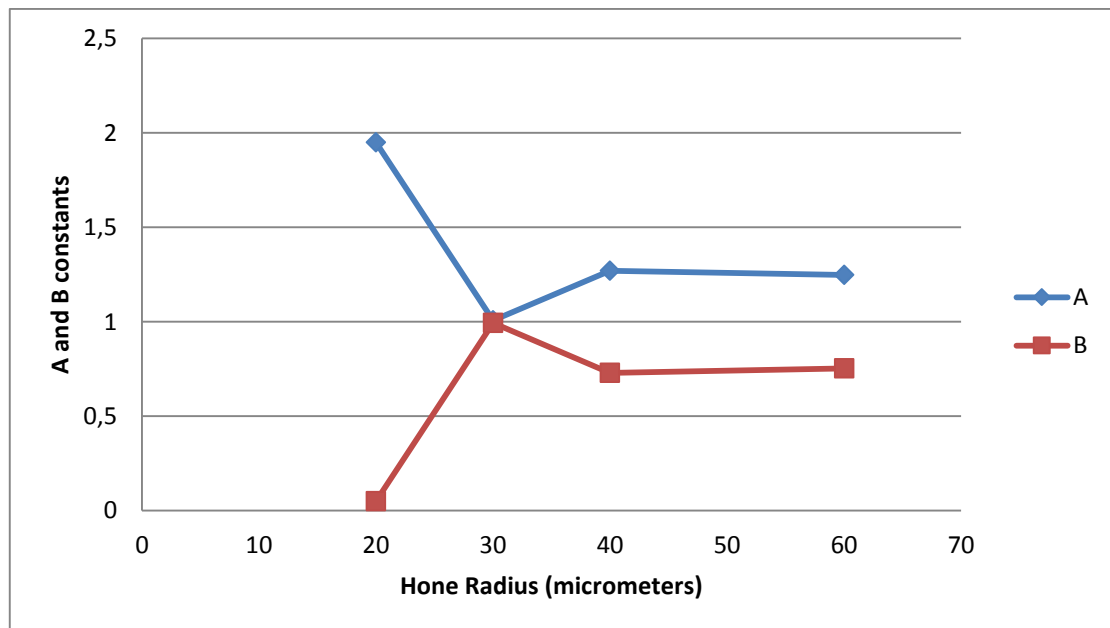


Figure 26 – Hone radius (micm.) vs a and b

The a and b values are derived as a function of hone radius of the cutting edge of the tool as;

$$a = -0,011 * honeradius + 1,815 \quad (3.35)$$

$$b = 0,0011 * honeradius + 0,184 \quad (3.36)$$

After the contact length prediction model is derived, the *P*MAX value illustrated on Figure 18 will be calibrated according to the contact length predictions. The calibrated (*P*MAX/*P*0) constants are shown in Table 5.

Hone (micm.)	Feed (mm/rev)	Cutting S. (m/min)	Exp. Con. L. (microm.)	Mod. Con. L. (microm.)	pmax/p0
60	0,2	250	147	158,6	1,15
60	0,15	250	116	140,9	1,15
60	0,1	250	114	108,5	1,15
40	0,2	250	98,8	108,27	1,31
40	0,15	250	89,64	108,14	1,31
40	0,1	250	92,83	101,88	1,31
30	0,2	250	57	84,2	1,38
30	0,15	250	60	84,2	1,38
30	0,1	250	70	89,2	1,38
20	0,2	250	62,48	58,2	1,73
20	0,15	250	74,32	58,2	1,73
20	0,1	250	79,83	58,2	1,73

Table 5 – P*MAX* / P0

The change on (*P*MAX/*P*0) according to the change of hone radius is shown in Figure 27.

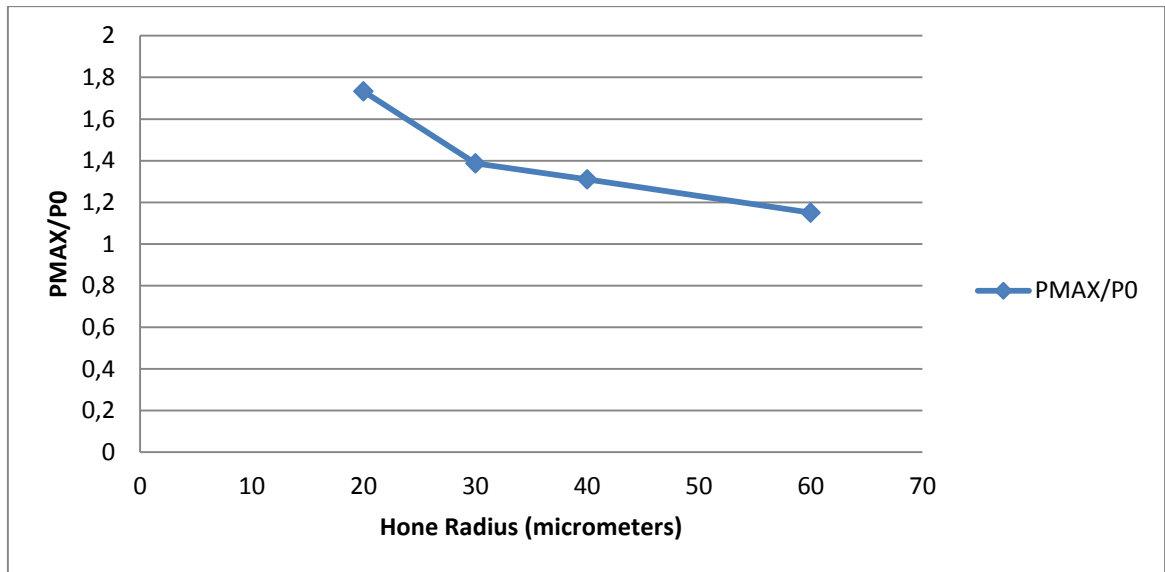


Figure 27 – Hone Radius (microm.) vs PMAX/P0

The ($PMAX/P0$) is written as a function of hone radius (microm.) as in (3.37).

$$PMAX/P_0 = -0.013 * honeradius + 1.891 \quad (3.37)$$

After the ($PMAX/P0$) is modeled, the modeling of third deformation zone is completed. The comparison of cutting force results for experiment results and simulation results are illustrated on Figure 28 and Figure 29.

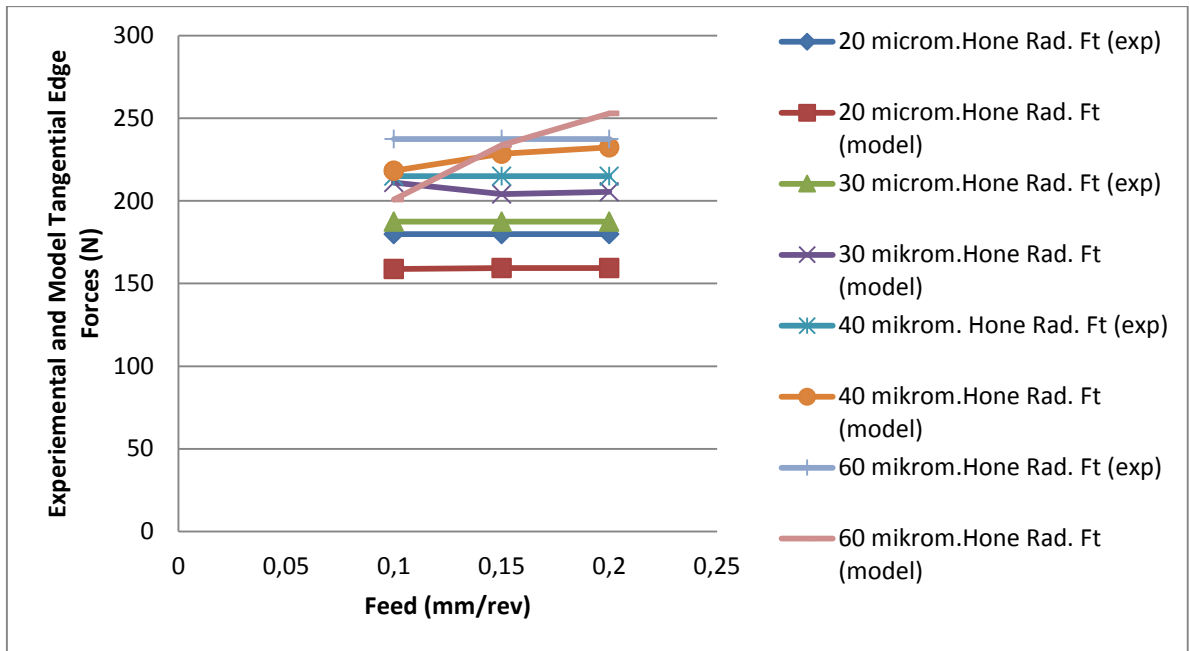


Figure 28 – Feed (mm/rev) vs tangential edge forces Ft (N)

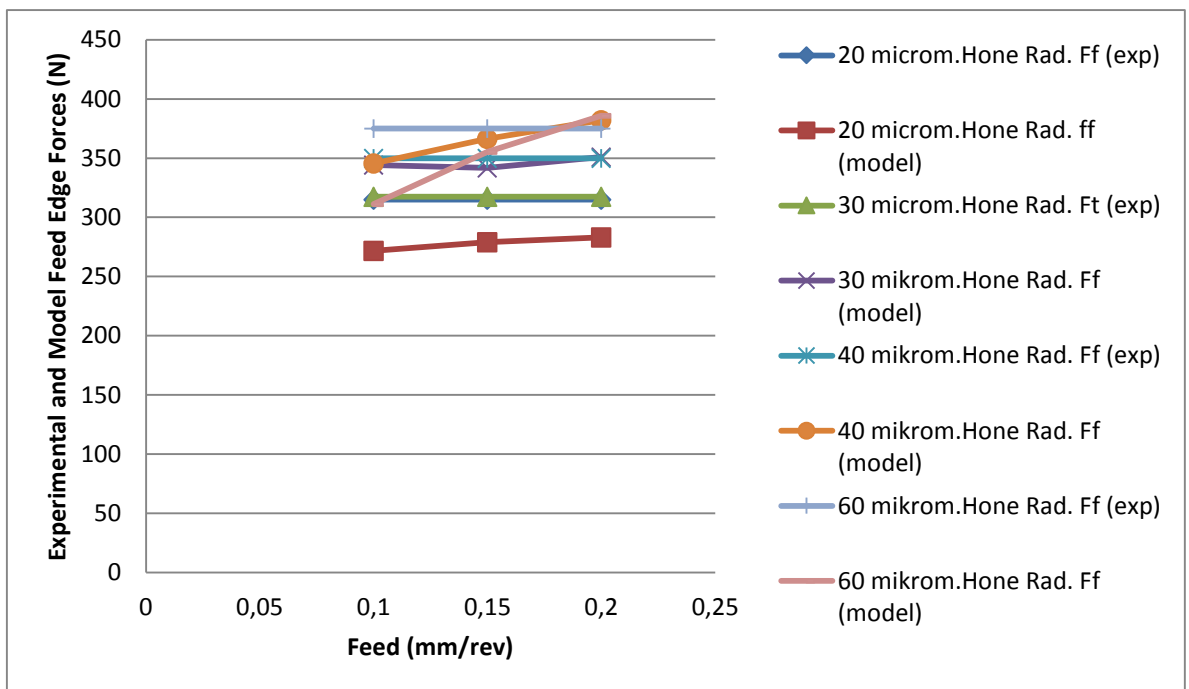


Figure 29 – Feed (mm/rev) vs feed edge forces Ff (N)

3.3. Experimental Modeling of Third Deformation Zone in Micro End Milling Operations

In this part of the thesis the force model developed for the third deformation zone will be introduced into micro end milling operations. For consistency between the directions of the forces, the model is developed for the regions illustrated on

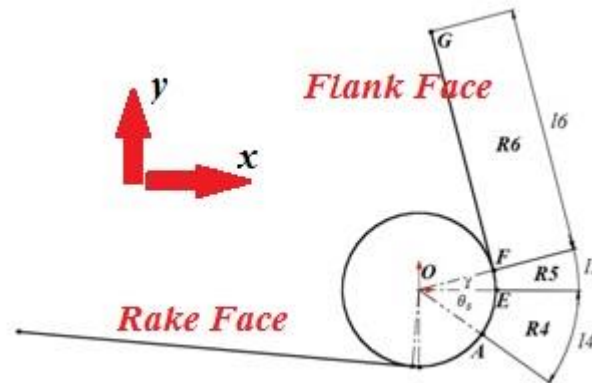


Figure 30 - Cutting Regions on the Flank Face

The axial depth of cut is divided with the same finite number of elements as it was discussed in Chapter 2 and total forces exerted on the tool due to the third deformation zone is calculated by summing up the forces on each element. As the mathematical formulations for the modeling was described earlier in this Chapter, the model will not be described in here.

3.4. Experimental Investigation of Third Deformation Zone Forces

As it was discussed earlier, the third deformation zone appears due to the hone radius at the cutting edge of the tool. The flank face of the cutting tool always has a contact with the newly formed surface and due to that contact which is considered as ploughing or in other words the rubbing affect, some forces are exerted on the cutting tool. One of the most important aspect of the third deformation zone is, there is no chip formation occurs in the region, the chip formation is due to the plastic deformation on the secondary deformation zone on the rake face. On the other hand, there appears a minimum or

critical uncut chip thickness value on the cutting operations due to the hone radius. The chip will not be generated if the uncut chip thickness is less than this critical value [26]. Even though the chip will not be generated when the uncut chip thickness is less than this critical value, the third deformation zone forces are still exerted on the cutting tool. Therefore understanding the mechanism of the critical uncut chip thickness is important for the third deformation zone analysis. There are various approaches have been used in order to determine and model this critical uncut chip thickness value. In their work, Liu *et al.* [26] developed an analytical model to predict the critical uncut chip thickness value while considering the thermal softening and strain hardening effects. Yuan *et al.* [27] experimentally studied on the subject and they estimated the minimum uncut chip thickness as between 20% and 40% of the cutting edge radius. Vogler *et al.* [16] worked on finite element analysis in microstructure level and found that the critical uncut chip thickness to edge radius ratio as 0.20 for pearlite and 0.35 for ferrite.

It was also described earlier in the thesis that, the uncut chip thickness varies as a function of immersion angle of the cutting edge of the tool in milling operations. The uncut chip thickness can be described as a function of the feed per tooth and immersion angle as follows;

$$h(\phi) = c \sin \phi \quad (3.37)$$

where c is the feed per tooth (mm/rev.tooth) and ϕ is the instantaneous angle of immersion [5]. When we consider a half immersion up-milling operation, the immersion angle of the cutting edge of the tool starts with 0 degrees and the tool edge exits the workpiece with 90 degrees immersion angle. When we consider the situation in uncut chip thickness perspective, the uncut chip thickness starts with a value of 0 and rises until the immersion angle reaches 90 degrees which lead to the maximum uncut chip thickness value. When we consider the variable chip thickness feature of the milling operations and the minimum uncut chip thickness analogy together, there should appear a critical immersion angle which defines the minimum uncut chip thickness value. The forces exerted on the cutting edge of the tool must be due to the third deformation zone when the actual immersion angle is less than this critical value. As the tool rotates and the immersion angle increases and the chip formation starts and the forces exerted on

the cutting edge of the tool must be due to primary, secondary and third deformation zones. The described situation is illustrated on Figure 31.

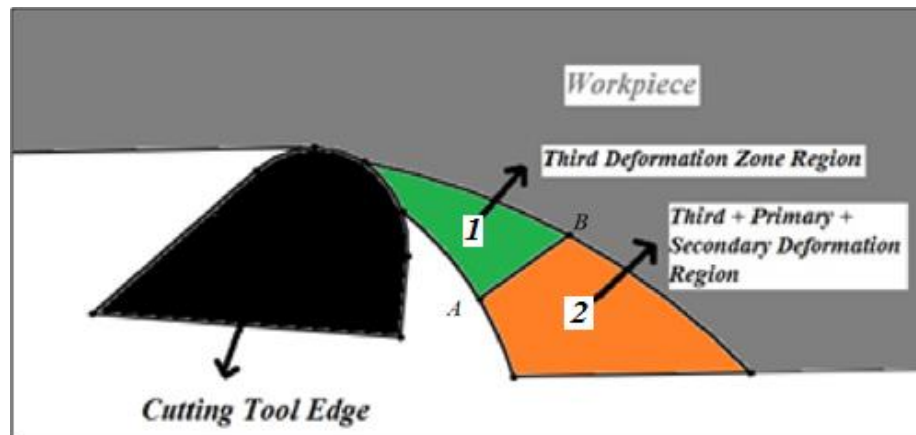


Figure 31 - Minimum Uncut Chip Thickness in Upmilling Operations

If the line between the points A and B on Figure 31 considered as the minimum uncut chip thickness, the region illustrated as 1 or in green color, is the zone where no chip formation occurs. The forces exerted on the cutting edge of the tool are due to the third deformation zone which is governed by the ploughing mechanism. As the tool rotates and passes the line between the points A and B on Figure 31, the uncut chip thickness gets larger than the minimum uncut chip thickness value and therefore in the region illustrated as 2 or in orange color, is the zone where chip formation starts. The forces exerted on the cutting edge of the tool in this region are due to the primary, secondary and third deformation zones. It is expected that there should be a transition point on the cutting forces which is due to the transition on the critical immersion angle which defines the minimum uncut chip thickness value.

The break points or in other works transition points on the cutting forces were investigated experimentally. The experiments were carried out on KERN Evo Ultra Precision CNC Machining Centre which has 0.1 μm resolution and $\pm 1.0 \mu\text{m}$ positioning tolerance. The machining centre is shown in Figure 32. Kistler Type 9256C dynamometer shown in Figure 34 is used during the experiments. Cutting tool that was used in the experiments has 6 mm diameter, 12 μm hone radius, 5 degree helix angle and 7 degree clearance angle with 4 teeth. The cutting tool is illustrated on Figure 33.

The workpiece material used during the experiments is AISI 1050 Steel. The cutting parameters used in the experiments are shown in Table 6.

Axial Depth of Cut (mm)	Radial Depth of Cut (μm)	Cutting Speed (m/min)	Feed (mm/rev*t)
2	200	95	0.001-0.003-0.005-0.007-0.009-0.011-0.013-0.015-0.017-0.019-0.021-0.023-0.025-0.027-0.029-0.031-0.033-0.035-0.037-0.039-0.041-0.043-0.045-0.047

Table 6 – Cutting Conditions for Third Deformation Zone Experiments



Figure 32 – KERN Evo Ultra Precision Machining Centre



Figure 33 – The Cutting Tool used in third deformation zone analysis



Figure 34 – Kistler Type 9256C

The measurements were carried out with 100,000 samples per second. The reason of usage high sampling rate is to be able to catch the transition point on the experimental data. A sample cutting test data is illustrated on Figure 35. The x axis of the graph represents the instantaneous immersion angle of the cutting tool and the y axis represents the forces in feed and the tangential directions. The transition angle is clearly observed and indicated on the figure as a red line where the break point on the forces occurs. The left side of the transition angle responds to only third deformation zone forces and the right side of the transition angle responds to third, primary and the secondary deformation zones forces. The same analysis carried out on each of the experimental data shown in Table 7. The forces at the transition angles for each of the experiments are shown in Figure 36.

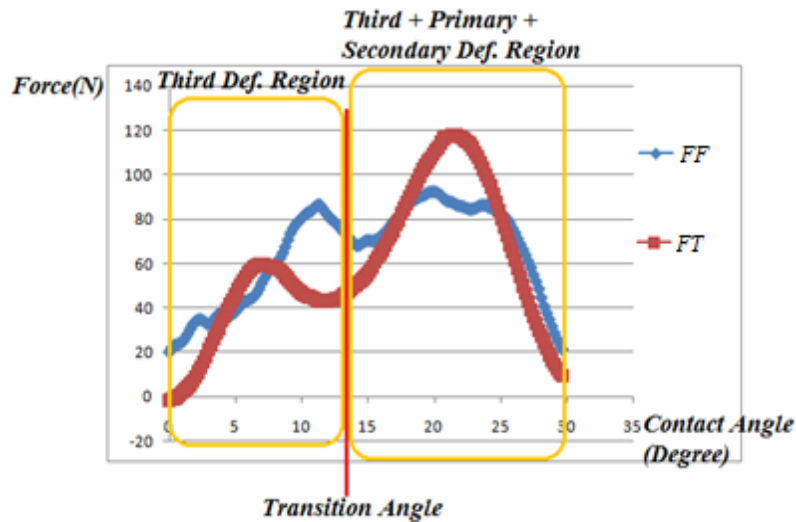


Figure 35 – Third Deformation Zone Analysis with 0.021 mm/rev*t feed, 6 mm diameter cutting tool, 5 degree helix angle, 2 mm axial depth of cut, 0.2 mm radial depth of cut, 5000 rpm spindle speed

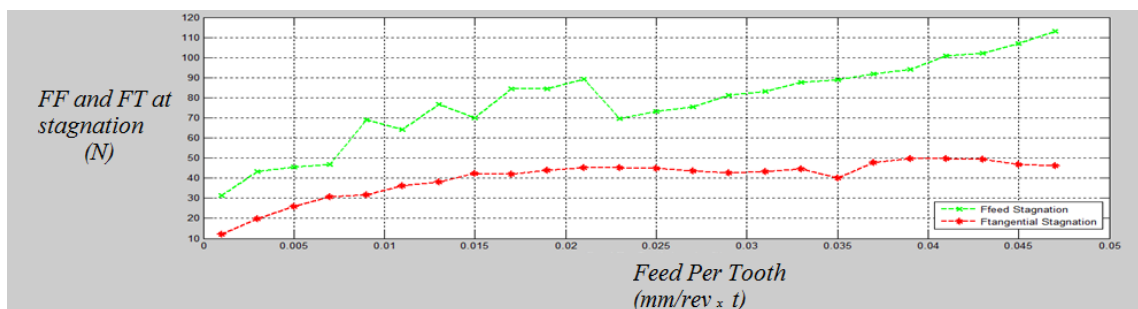


Figure 36 – Feed per Tooth vs Feed (green lines) and Tangential (red lines) Forces at the stagnation angle

The third deformation zone cutting coefficients are taken as the average of the cutting forces on the transition point. The coefficients for the feed and the tangential direction are derived as in Table 7.

Kfedge (N/mm)	Ktedge (N/mm)
39,03	20,04

Table 7 – Third Deformation Zone Force Coefficients derived experiemntally

4. EXPERIMENTALLY INVESTIGATION OF THE BOTTOM EDGE FORCES IN MICRO END MILLING OPERATIONS

The bottom edge forces in milling operations appear due to the contact between the newly formed surface at the axial depth and the bottom edge of the cutting tool. Even though this contact does not contribute to the chip formation, there exist appear some forces acting on the cutting tool. In order to investigate the effect of the bottom edge contact on the total cutting forces two sets of experiments were conducted. The first experimental setup is designed as the bottom edge of the cutting tool does not have any contact with the newly formed surface. On the other hand the second experimental setup is designed as a regular slot milling operation in which the bottom edge of the cutting tool is in contact with the newly formed surface. The illustrations of these experimental setups are shown in Figure 37.

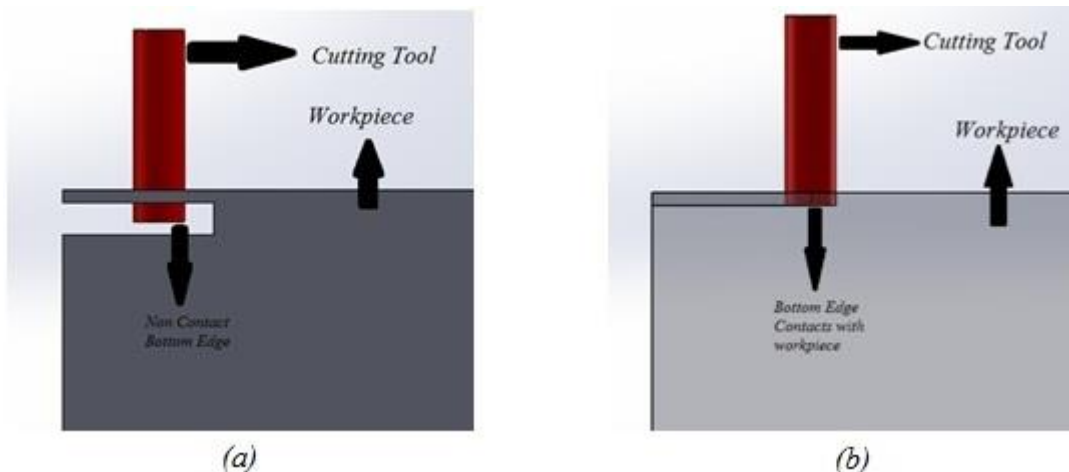


Figure 37 – (a) First experimental setup, bottom edge has no contact with the newly formed surface, (b) Second experimental setup, bottom edge has a contact with the newly formed surface

The bottom edge forces are calibrated where the coefficients are identified through experiments. For the two experiment sets, exactly the same cutting parameters were used. In the tests a solid carbide cutting tool with 2 mm diameter and 30 degree helix angle was used. The material of the workpiece on which the tests are conducted is AISI 1050 steel. 18 experiments were conducted with non-contact and contact cases. The spindle speeds were chosen as (7000, 8000, 9000, 10000, 11000, 12000, 13000, 14000, 15000 (rpm)) and the feeds are (0.008 and 0.012 (mm/rev*t)). The cutting coefficients are derived using a calibration procedure which is summarized as;

Step1. Non-Contact Tests are made as shown in Figure 37(a).

Step2. Bottom Contact Tests are made as shown in Figure 37(b).

Step3. F_x and F_y are gathered from the dynamometer.

Step4. F_{feed} and $F_{tangential}$ are identified for each test and for instantaneous angle of immersion of the cutting edge of the tool.

Step5. The difference between F_{feed} and $F_{tangential}$ got the tests with bottom contact and no contact is determined for each instantaneous immersion angle.

Step6. The average of the force differences for each test pair is determined.

Step7. The change of the average difference for different spindle speeds (cutting speeds) are calculated and shown in Figure 38 and Figure 39.

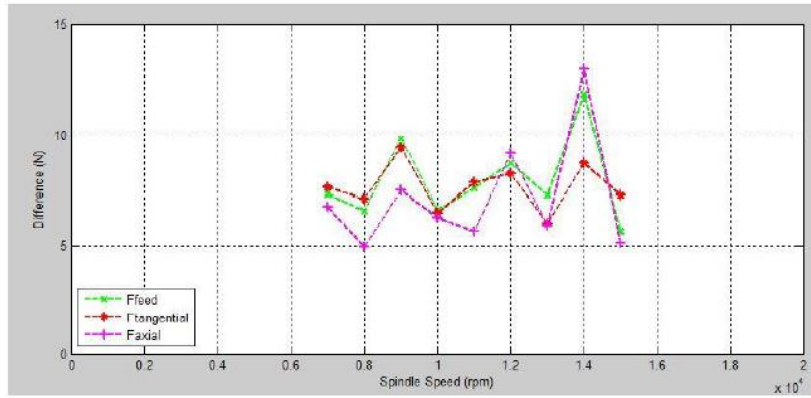


Figure 38 – Spindle Speed vs Ave. Diff. For Ffeed and Ftangential (f:0.008mm/rev*t)

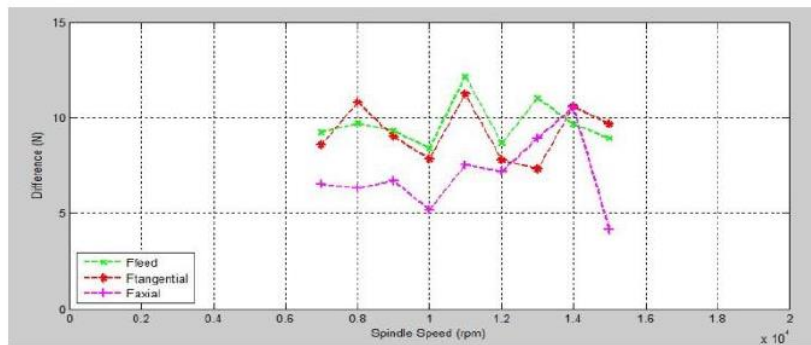


Figure 39 – Spindle Speed vs Ave. Diff. For Ffeed and Ftangential (f:0.012mm/rev*t)

The bottom edge coefficients are calibrated with respect to cutting speed as in Table 8.

KfBottomEdge (N.m/min)	KtBottomEdge (N.m/min)
0.16	0.17

Table 8 – Bottom Edge cutting coefficients

5. WORKING AND VERIFICATION OF THE PROPOSED MODELS

In this chapter of the thesis the working of the proposed models which are for primary, secondary and third deformation zones and bottom edge forces will be discussed in detail. Later, the model results will be compared with the experiments. The total cutting forces in feed and tangential directions are calculated as;

$$F_{Feed} = F_{F Primary} + F_{F Secondary} + F_{F Third} + F_{F Bottom} \quad (5.1)$$

$$F_{Tangnetial} = F_{T Primary} + F_{T Secondary} + F_{T Third} + F_{T Bottom} \quad (5.2)$$

The solution procedures for the cutting forces are summarized as in Figure 40.

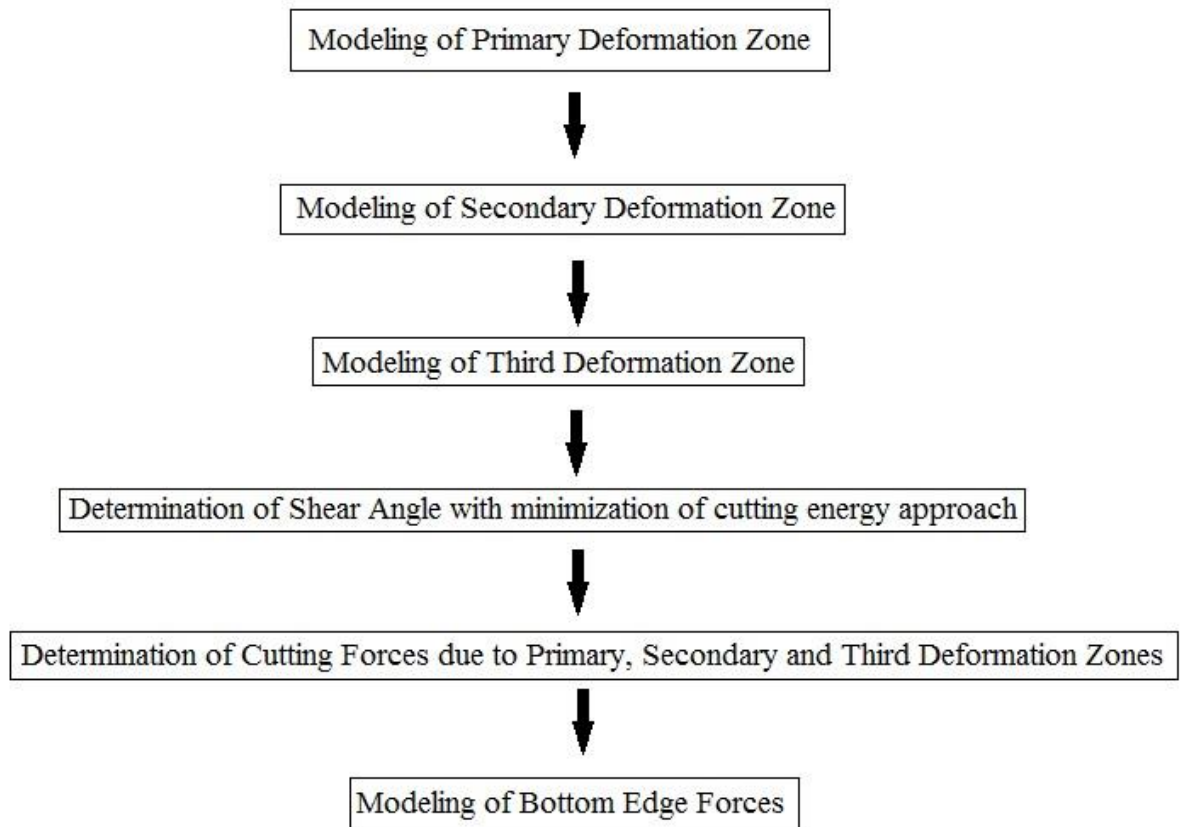


Figure 40 – Solution steps for proposed model

5.1. Working of Proposed Models

The details of the working of the proposed models listed on Figure 40 will be discussed in this part of the chapter.

5.1.1. Primary Deformation Zone

As it was described in Equation (2.3), the primary deformation zone is modeled with Johnson – Cook constitutive material model. The primary deformation zone is assumed to be a shear band which has a constant thickness, the thickness of the shear band is taken as $2.5\mu\text{m}$. All the experiments made to verify the proposed models were conducted on AISI 1050 steel. The Johnson – Cook material constants for AISI 1050

steel were taken from works in the literature [22]. The material constants are listed as in Table 9.

A (MPA)	B (MPA)	n	m	v
880	500	0,234	0,0134	1

Table 9 – Johnson – Cook parameters for the proposed model for AISI 1050 steel

The shear stress at the beginning of the primary deformation zone is calculated iteratively from Johnson – Cook constitutive material model by using Runge – Kutta mathematical iteration method. After the shear stress at the beginning of the primary deformation zone is determined, the shear stress at the end of the shear band is calculated as in Equation (2.5). The shear stress at the end of the shear band is later used in rake contact analysis which will be discussed later.

5.1.2. Secondary Deformation Zone

The secondary deformation zone is modeled with Two-Zone Contact model. The sliding friction coefficient is determined by the equation calibrated for workpiece and tool pair. The sliding friction coefficient is taken from [22] for AISI 1050 steel and coated carbide tool as;

$$\mu_s = 0.8932 + 1 \times 10^{-6} V^2 - 0.0016 V \quad (5.3)$$

in which V is the cutting speed in (m/min).

The total contact length is calculated with an iterative approach and an initial value for the total contact length is taken as in Equation (2.11). The assumption on the iterations depends on the fact that, the moment at the tip of the cutting edge of the tool is equal to

0. The sticking zone contact length is determined from the Equation (2.10). The normal and the friction forces are determined from the Equations (2.17) – (2.35)

5.1.3. Third Deformation Zone

The third deformation zone is modeled with the same thermo-mechanical approach that was discussed for the secondary deformation zone. Even though the same approach the same approach was used, the normal pressure distribution is assumed to be as in Figure 18. The total contact length in third deformation zone is taken from the experiments made in literature [23]. The sticking zone contact length is equal to (2.10s). The P_{MAX} is chosen as in Figure 27, where P_0 is derived from the secondary deformation zone analysis as in Equation (2.13). The normal and friction forces acting on third deformation zone is calculated as in Equations (3.10) – (3.33).

5.1.4. Bottom Edge Forces

As the details of the determination of bottom edge forces were discussed in details in Chapter 4, the investigations will not be given in this Chapter.

5.2. The Experimental Verification

The cutting experiments were conducted on AISI 1050 steel. The machine that was used in experiments was Kern Evo Ultra Precision Machining Center shown in Figure 32. The forces were derived with Kistler 9256 C dynamometer shown in Figure 34. The cutting tool that was used in the experiments has 30 degree helix angle, 5 degree rake angle and 3 degree clearance angle. The hone radius of the cutting tool was 8 micrometers and the hone radius was derived with Nanofocus USurf microscope shown in Figure 41. The tool has 0.8 mm diameter. The experiments were made as a slotting operation, the axial depth of cut and spindle speed was kept constant as 0.1mm and 5000 rpm respectively. There were 10 different feeds were used in the experiments which are (0.075, 0.078, 0.8, 0.83, 0.85, 0.88, 0.9, 0.93, 0.095 and 0.098). The comparisons of the experiment and simulation results are shown in Figure 42.



Figure 41 – Nanofocus Usurf

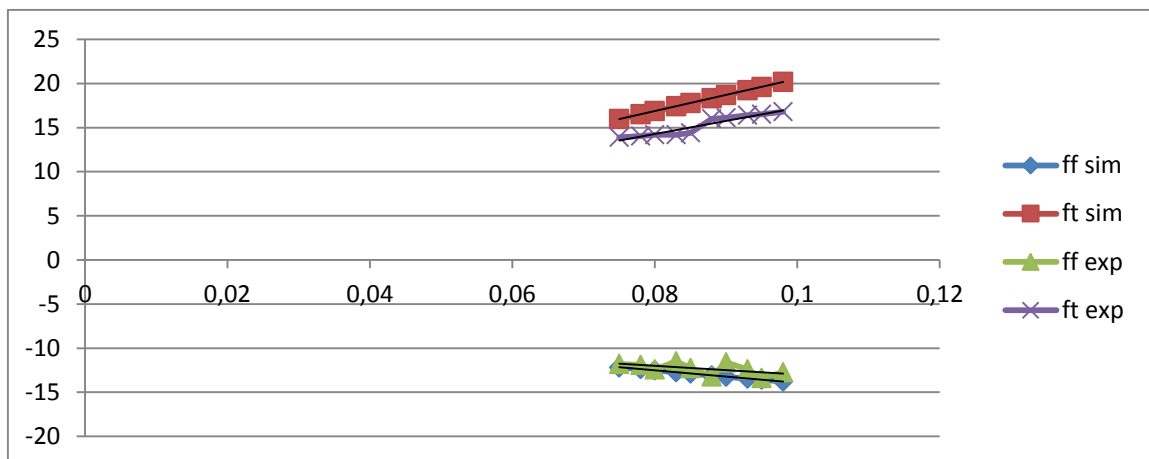


Figure 42 – Cutting test results for the forces in feed and tangential directions

Another set of experiments were also carried out with the same diameter cutting tool. In the next experimental setup, two different axial depths of cuts (0.1 and 0.2 mm) were used. The experiments were made as a slotting operation with 10 micrometers hone radiused cutting tool. The spindle speed was kept constant as 5000 rpm during the experiments. The experiment results are illustrated in Figure 43 and Figure 44.

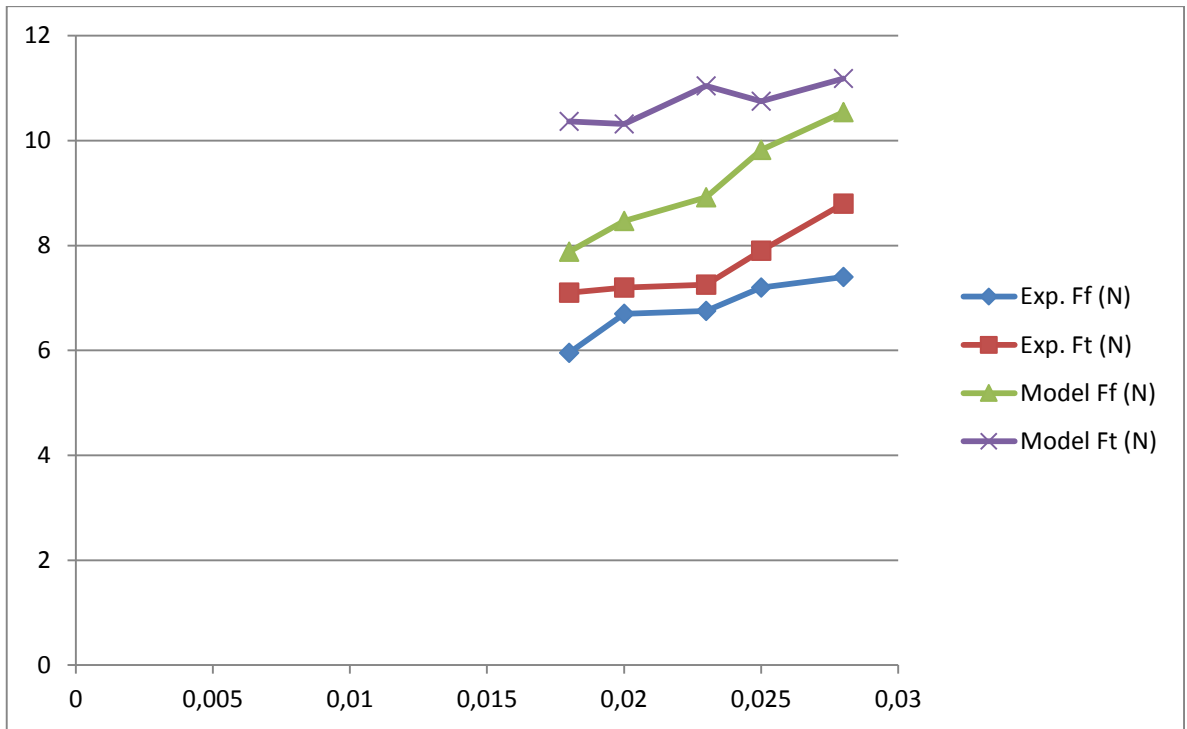


Figure 43 – Feed (mm/rev*t) vs experiment and model results for the forces in feed and the tangential directions

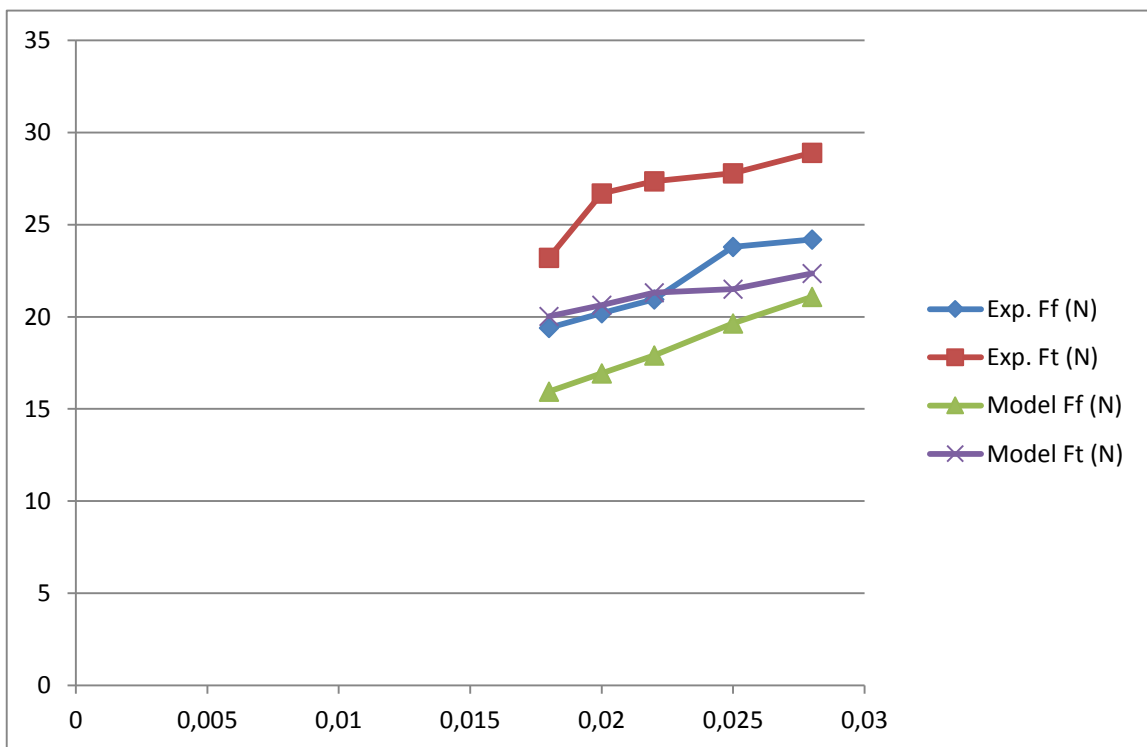


Figure 44 – Feed (mm/rev*t) vs experiment and model results for the forces in feed and the tangential directions

As it can be observed from the Figure 43 and Figure 44, the model predicts the forces for micro end milling operations which a small and acceptable difference with the experimental results. As it can also be observed from the figures the model predicts the forces higher than the experimental results for all of the cases. The main reason for this difference might be due to the material model which was made for the primary deformation zone analysis.

6. SUGGESTIONS FOR FURTHER RESEARCH

Following are the recommended studies for extending the capabilities of the presented models in this study;

- The primary deformation zone is modeled via Johnson – Cook constitutive material model. The model works well for conventional orthogonal, oblique and milling operations. However as the cutting occurs in a relatively small area for micro – milling operations another material model designed for specifically micro and nano scales might be used.
- While modeling the milling analogy the axial depth of cut is divided into a finite number of elements in order to consider the variable uncut chip thickness property of the milling operations. Instead of dividing the axial depth of cut, the uncut chip thickness might be written as an integrating function of axial depth of cut and this might reduce the computation time of the simulations.
- The friction coefficients derived for micro-milling operations are calibrated for orthogonal cutting case and plugged into micro-milling, that might be one of the results for the discrepancy between the model and experimental results.
- The third deformation zone is modeled via thermo-mechanical approach and the normal pressure distribution in the third deformation zone is modeled as a parabolic function. The behavior of the normal pressure in the third deformation zone should also be investigated experimentally.
- The contact lengths in the third deformation zone are calibrated through the experiments taken from the literature just for one cutting speed. The number of experiments made for the third deformation zone contact length analysis should be increased and the full recovery and partial recovery models which were discussed in Chapter 3 should be updated accordingly.

- The bottom edge cutting forces are calculated by experimentally calibrated coefficient by using a mechanistic approach. The mechanistic approach gives good results for a certain range of cutting parameters however the coefficients need to be recalculated for different cutting parameters as well which needs an important effort. So instead of using a mechanistic approach for the bottom edge forces, the region might be modeled by a thermo-mechanical approach as in the third deformation zone.

7. DISCUSSIONS AND CONCLUSIONS

In this thesis, the cutting forces in milling and orthogonal cutting operations are derived by using models developed by thermo-mechanical and mechanistic approaches. All of the proposed models throughout the thesis are verified through the experiments. The primary, secondary and third deformation zones in cutting operations are modeled with the thermo-mechanical approach. The primary deformation zone is modeled via Johnson – Cook constitutive material model which considers the behavior of the material under high temperature. The secondary deformation zone is firstly modeled using the Dual – Zone contact model [22]. For the third deformation zone, there were two different approaches have been used. Firstly, the forces due to the third deformation zone are calculated with the thermo-mechanical approach. Secondly, a new experimental procedure is developed for milling operations to directly identify the third deformation zone forces from only a single experiment data. With this new experimental approach as well as the third deformation zone forces, the minimum uncut chip thickness and stagnation angle can also be determined just from a single experiment. For the bottom edge forces, the cutting coefficients are calibrated and the a mechanistic model which calculates the bottom edge forces with the cutting coefficient is derived.

Specific contributions of the presented study are listed as follows;

- The thermo-mechanical approach is introduced into the micro – milling operations. By using the thermo-mechanical approach while modeling the

cutting forces, the number of calibration tests needed is decreased significantly. The calibration tests are only made for a tool and a workpiece pair and it can be used for a large range of cutting parameters.

- The third deformation zone which has a great contribution on the total cutting forces especially for the micro – milling operations are calibrated with the thermo-mechanical approach as well.
- With the newly developed experimental procedure for third deformation zone forces discussed in Chapter 3, the insight of the ploughing mechanism can be investigated in detail. As well as the edge forces, the stagnation angle and minimum uncut chip thickness can be identified just from a single cutting experiment.
- The bottom edge forces in milling operations are investigated experimentally and a mechanistic model is developed for identification of the cutting coefficients for the bottom edge forces.

REFERENCES

- [1] Woodbury, R. S., 1972, History of the Milling Machine. In Studies in the History of the Machine Tools, Cambridge, Massachusetts, USA and London, England: MIT Press.
- [2] Martellotti, M. E., 1941, An Analysis of the Milling Process, *Transactions of the ASME*, 63: 677 – 700.
- [3] Martellotti, M. E., 1945, An Analysis of the Milling Process, Part: II: Down Milling, *Transactions of the ASME*, 67: 233 – 251.
- [4] Budak, E., Altintas, Y., Armarego, E. J. A., 1996, Prediction of Milling Force Coefficients from Orthogonal Cutting Data, *Journal of Manufacturing Science and Engineering*, Vol. 118/ pg. 216 – 224.
- [5] Altintas, Y., 2000, Manufacturing Automation: Metal Cutting Mechanics, Machine Tool Vibrations, and CNC Design, Cambridge University Press.
- [6] Chae, J., Park, S. S., Freiheit, T., 2006, Investigation of Micro Cutting Operations, *International Journal of Machine Tools*, Vol. 46/ pg. 313 – 332.
- [7] Bissacco, G., Hansen, H. N., Slunsky, J., 2008, Modeling the Cutting Edge Radius Size Effect for Force Prediction in Micro Milling, *CIRP Annals – Manufacturing Technology*, Vol. 57/ pg. 113 – 116.
- [8] Jin, X., Altintas, Y., 2011, Slip – line Field Model of Micro – Cutting Process with Round Tool Edge Effect, *Journal of Materials Processing Technology*, Vol. 211/ pg. 339 – 355.
- [9] Fang, N., 2003, Slip – Line Modeling of Machining with a Rounded Edge Tool, Part I: New Model and Theory, *Journal of Mechanics and Physics of Solids*, Vol. 51/ pg. 715 – 742.
- [10] Altintas, Y., Jin, X., 2011, Mechanics of Micro – Milling with Round Edge Tools, *CIRP Annals – Manufacturing Technology*, Vol. 60/ pg. 77 – 80.

- [11] Malekian, M., Park, S. S., Jun, M. B. G., 2009, Modeling of Dynamic Micro – Milling Cutting Forces, *International Journal of Machine Tools and Manufacture*, Vol. 49/ pg. 586 – 598.
- [12] Park, S. S., Malekian, M., 2009, Mechanistic Modeling and Accurate Measurement of Micro End Milling Forces, *CIRP Annals – Manufacturing Technology*, Vol. 58/ pg. 49 – 52.
- [13] Bao, W. Y., Tansel, I. N., 2000, Modeling Micro – End Milling Operations. Part I: Analytical Cutting Force Model, *International Journal of Machine Tools and Manufacture*, Vol. 49/ pg. 2155 – 2173.
- [14] Newby, G., Venkatachalam, S., Liang, S. Y., 2007, Empirical Analysis of Cutting Force Constants in Micro End Milling Operations, *Journal of Materials Processing Technology*, 192 – 193 / pg. 41 – 47.
- [15] Zaman, M. T., Anantharajan, S. K., 2006, A three – dimensional Analytical Cutting Force Model for Micro End Milling Operations, *International Journal of Machine Tools and Manufacture*, Vol. 46/ pg. 353 – 366.
- [16] Vogler, M. P., Kapoor, S. G., DeVor, R. E., 2005, On the Modeling and Analysis of Machining Performance in Micro – Endmilling, Part II: Cutting Force Prediction, *Journal of Manufacturing Sciences and Engineering*, Vol. 126/ pg. 695 – 705.
- [17] Afazov, S. M., Ratchev, S. M., Segal, 2010, J., Modeling and Simulation of Micro – Milling Cutting Forces, *Journal of Materials Processing Technology*, Vol. 210/ pg. 2154 – 2162.
- [18] Jin, X., Altintas, Y., 2012, Prediction of Micro – Milling Forces with Finite Element Method, *Journal of Materials Processing Technology*, Vol. 212/ pg. 542 – 552.
- [19] Laia, X., Lia, H., Lia, C., Lina, Z., Nib, J., 2008, Modeling and Analysis of Micro Scale Milling Considering Size Effect, Micro Cutter Edge Radius and Minimum Chip Thickness, *International Journal of Machine Tools and Manufacture*, Vol. 48/ pg. 1 – 14.
- [20] Dang, J., Zhang, W., Yang, Y., Wan, M., 2010, Cutting Force Modeling for Flat End Milling Including Bottom Edge Cutting Effect, *International Journal of Machine Tools and Manufacture*, Vol. 50/ pg. 986 – 997.

- [21] Wan, M., Zhang, W., Yang, Y., 2011, Phase Width Analysis of Cutting Forces Considering Bottom Edge Cutting and Cutter Runout Calibration in Flat End Milling of Titanium Alloy, *Journal of Materials Processing Technology*, Vol. 211/ pg. 1852 – 1863.
- [22] Ozlu, E., Budak, E., 2007, Thermomechanical Modeling of Orthogonal Cutting Including the Effect of Stick – Slide Regions on the Rake Face, 10th CIRP International Workshop on Modeling of Machining Operations, Calabria, Italy, August.
- [23] Celebi, C., Ozlu, E., Budak, E., 2013, Modeling and Experimental Investigation of Edge Hone and Flank Contact Effects in Metal Cutting, 14th CIRP Conference on Modeling of Machining Operations, *Procedia CIRP* 8/ pg. 194 – 199.
- [24] Molinari, A., Dudzinski, D., 1992, Stationary Shear Bands in High Speed Machining, *Comptes Rendus Acad. Sciences*, 315, Série II, 399 – 405.
- [25] Dudzinski, D., Molinari, A., 1997, A Modeling of Cutting For Viscoplastic Materials, *International Journal of Mech. Sci*, 39/4: 369 – 389.
- [26] Liu, X., DeVor, R. E., Kapoor, S. G., 2005, An Analytical Model for the Prediction of Minimum Chip Thickness in Micromachining, *Journal of Manufacturing Sciences and Engineering*, Vol. 128/ pg. 474 – 481.
- [27] Yuan, Z. J., Zhou, M., Dong, S., 1996, Effect of Diamond Tool Sharpness on Minimum Cutting Thickness and Cutting Surface Integrity in Ultraprecision Machining, *Journal of Materials Processing Technology*, Vol. 62/ pg. 327 – 330.